Materials Today Sustainability 26 (2024) 100733

Contents lists available at ScienceDirect

Materials Today Sustainability

journal homepage: www.journals.elsevier.com/materials-today-sustainability

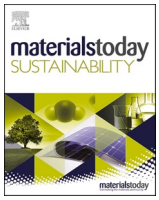

Exploring the potential of transition-metal-based hollow micro- and nanoparticles in supercapacitor electrodes

Pooria Tajalli [a], Mina Omidiyan [a], M. Mim Rahimi [b,*], T. Randall Lee [a,**]

[a] Department of Chemistry and Texas Center for Superconductivity, University of Houston, Houston, TX 77204, United States
[b] Department of Civil and Environmental Engineering and Materials Science & Engineering Program, University of Houston, Houston, TX 77204, United States

ARTICLE INFO

Keywords:
Supercapacitors
Hollow nanoparticles
Transition metal oxides (TMOs)
Transition metal sulfides (TMSs)
Transition metal phosphides
Transition metal phosphates (TMPs)
Transition metal selenides (TMSes)

ABSTRACT

The development of high-performance supercapacitors for energy storage applications is important in the era of renewable energy. This review article comprehensively analyzes the electrochemical performance of transition metal-based hollow micro- and nanoparticles, including transition metal oxides (TMOs), transition metal sulfides (TMSs), transition metal phosphides/phosphates (TMPs), and transition metal selenides (TMSes). The study focuses on specific capacitance, energy density, power density, and cycling stability. In addition, this study investigates the impact of various properties of micro- and nanoparticles on the electrochemical performance of supercapacitors. These properties include morphology, shell thickness, pore size, porosity, crystallinity, metallic and non-metallic element ratio, and incorporation of conductive materials such as carbon or conductive polymer into their structures. The analysis finds that TMPs exhibit the highest specific capacitance due to their high theoretical capacitance. Furthermore, the review also highlights the significance of employing transition metal-based materials as both anode and cathode to achieve a high energy density. The highest energy density was observed in the TMSe-based supercapacitor constructed from pseudocapacitive cathode and anode. The study provides valuable insights into the current research landscape of transition metal-based hollow micro- and nanoparticles and sheds light on areas that may require further investigation. Ultimately, this review contributes to the development of high-performance supercapacitors and could aid in realizing their full potential in energy storage applications.

1. Introduction

To ensure stable power output to the grid from renewable sources, energy storage plays an essential role. Among the various energy storage technologies being explored, batteries have been widely used for energy storage due to their high energy density and the ability to provide a stable power output over a long period of time [1–7]. Batteries have found their application in various devices such as cellphones, electric vehicles, and stationary energy storage [8–11]. However, applications that require high power density and fast charging/discharging rates, such as backup power supplies and portable electronic devices demand alternative energy storage technologies [12–15]. Supercapacitors (SCs) have emerged as a promising option due to their high power densities, fast charge/discharge rates, and long cycle lives [16–19,94]. SCs are particularly well-suited for the applications where high power densities and fast charge/discharge rates are required, such as in electric vehicles, backup power supplies, and portable electronic devices [12–15,20]. Despite their advantages, the lower energy density of SCs (1–10 Wh kg^{-1}) in comparison to batteries (10–100 Wh kg^{-1}) can restrict the range of their possible applications [21].

A supercapacitor typically consists of two electrodes separated by an electrolyte. The electrodes are often made of high-surface-area materials to store electric charge and the electrolyte facilitates the flow of ions between the electrodes [22]. SCs can be classified into two categories based on their charge storage mechanism: electric double layer capacitors (EDLCs) and pseudocapacitors (PCs) [16]. EDLCs store electrical charge on the electrode/electrolyte interface by creating an electric double layer [23]. These types of electrodes are mostly made from carbon-based materials, such as activated carbon and carbon nanotubes, due to their high specific surface area and good electrical conductivity [14,24,25]. However, EDLCs have relatively low specific capacitance and energy density, meaning they can store only a limited amount of

* Corresponding author.
** Corresponding author.
E-mail addresses: mrahimi@uh.edu (M.M. Rahimi), trlee@uh.edu (T.R. Lee).

https://doi.org/10.1016/j.mtsust.2024.100733
Received 2 October 2023; Received in revised form 2 February 2024; Accepted 6 March 2024
Available online 8 March 2024

Table 1
Electrochemical and morphological comparison between TMO hollow nanoparticle-based supercapacitors.

Metal	Composition	Morphology	Specific Capacitance	Energy Density	Cycling Stability	Ref.
Mn	MnO_2	Hollow nanofibers	291.0 F g^{-1} at 1.0 A g^{-1}	–	90.9% after 5000 cycles at 50.0 mV s^{-1}	[40]
	Mn_3O_4/rGO	Hollow multi-shelled microspheres	720.5 F g^{-1} at 1.0 A g^{-1}	112.0 Wh kg^{-1} at 850.0 W kg^{-1}	90% after 5000 cycles at 10.0 A g^{-1}	[47]
V	V_2O_5	Hollow nanospheres	723.1 F g^{-1} at 1.0 A g^{-1}	1.2 Wh m^{-2} at 4.0 W m^{-2}	37% after 100 cycles at 1.0 mA cm^{-2}	[48]
Ni	NiO	Hollow double-shelled nanospheres	473.0 F g^{-1} at 0.5 A g^{-1}	21.4 Wh kg^{-1} at 375.8 W kg^{-1}	92.3% after 3000 cycles at 5.0 A g^{-1}	[49]
	NiO	Hollow nanospheres	1058.0 F g^{-1} at 2.0 A g^{-1}	35.8 Wh kg^{-1} at 780.0 W kg^{-1}	86% after 3000 cycles at 2.0 A g^{-1}	[46]
	NiO/NC	Hollow nanospheres	1026.0 F g^{-1} at 1.0 A g^{-1}	40.2 Wh kg^{-1} at 750.2 W kg^{-1}	90.2% after 10000 cycles at 50.0 mV s^{-1}	[29]
Co	Co_3O_4	Hollow multi-shelled nanospheres	688.2 F g^{-1} at 0.5 A g^{-1}	–	93.2% after 2000 cycles at 2.0 A g^{-1}	[50]
	NC@Co_3O_4	Hollow nanospheres	581.0 F g^{-1} at 1.0 A g^{-1}	34.5 Wh kg^{-1} at 753.0 W kg^{-1}	100% after 5000 cycles at 5.0 A g^{-1}	[51]
	Co_3O_4/rGO/CM	Hollow nanospheres	1106.0 F g^{-1} at 1.0 A g^{-1}	66.7 Wh kg^{-1} at 750.0 W kg^{-1}	86.7% after 5000 cycles at 5.0 A g^{-1}	[52]
	Co_3O_4@PANI	Hollow nanopolyhedra	1301.0 F g^{-1} at 1.0 A g^{-1}	41.5 Wh kg^{-1} at 800.0 W kg^{-1}	83.4% after 5000 cycles at 5.0 A g^{-1}	[34]
Zn–Co	$ZnCo_2O_4$	Hollow microspheres	568.0 F g^{-1} at 1.0 A g^{-1}	27.8 Wh kg^{-1} at 158.5 W kg^{-1}	178% after 2000 cycles at 1.0 A g^{-1}	[53]
Ni–Co	NC@$NiCo_2O_4$	Hollow nanocubes	966.2 F g^{-1} at 1.0 A g^{-1}	41.9 Wh kg^{-1} at 750.4 W kg^{-1}	73.6% after 5000 cycles at 5.0 A g^{-1}	[35]
Co–Ce	Co_3O_4–CeO_2	Hollow nanopolyhedra	1288.3 F g^{-1} at 2.5 A g^{-1}	54.9 Wh kg^{-1} at 849.9 W kg^{-1}	98% after 6000 cycles at 4.0 A g^{-1}	[54]
Cu–Co	$CuCo_2O_4$	Hollow double-shelled nanospheres	1402.0 F g^{-1} at 2.0 A g^{-1}	38.4 Wh kg^{-1} at 800.0 W kg^{-1}	94.1% after 5000 cycles at 10.0 A g^{-1}	[55]
Co–V	V–Co_3O_4	Hollow multi-shelled nanospheres	1593.0 F g^{-1} at 0.3 A g^{-1}	66.9 Wh kg^{-1} at 240.0 W kg^{-1}	–	[43]
	$Co_3V_2O_8$	Hollow nanospheres	2376.0 F g^{-1} at 2.0 A g^{-1}	59.2 Wh kg^{-1} at 250.0 W kg^{-1}	97.3% after 10000 cycles at 20.0 A g^{-1}	[22]
Mn–Sn	MnO_2@SnO_2	Hollow nanospheres	541.6 F g^{-1} at 1.0 A g^{-1}	18.1 Wh kg^{-1} at 403.6 W kg^{-1}	86% after 2500 cycles at 0.5 A g^{-1}	[56]
Mn–Fe	$MnFe_2O_4$/rGO	Hollow nanospheres	768.0 F g^{-1} at 8.0 A g^{-1}	28.1 Wh kg^{-1} at 750.0 W kg^{-1}	95% after 4000 cycles at 1.0 A g^{-1}	[42]
Zn–Mn	$ZnMn_2O_4$	Hollow nanofibers	1026.0 F g^{-1} at 2.0 A g^{-1}	–	100.8% after 5000 cycles at 6.0 A g^{-1}	[57]

energy per unit weight [14,26]. The specific capacitance C_s (F g^{-1}) and energy density E (Wh kg^{-1}) of the SCs is calculated by Eq. (1) and Eq. (2), respectively,

$$C_s = \frac{I \times \Delta t}{m \times \Delta V} \quad \text{(Eq. 1)}$$

$$E = \frac{Cs \times (\Delta V)^2}{2 \times 3.6} \quad \text{(Eq. 2)}$$

where Q (C) is the quantity of electrical charge, m (g) is the mass of the electrode, I (A) is the current, Δt (s) is the discharge time, and ΔV (V) is the potential window. On the other hand, PCs stores electric charge via fast and reversible reduction-oxidation (redox) reactions at the surface and near the surface of the electrodes which provide higher specific capacitance and energy density compared to EDLCs [27,28]. PCs electrodes can be constructed from transition metal compounds such as transition metal oxides (TMOs) [29], transition metal sulfides (TMSs) [30], transition metal phosphides/phosphates (TMPs) [31], and transition metal selenide (TMSes) [13] owing to their high theoretical capacity [13,29–32]. Although transition metal compounds have higher specific capacitance compared to EDLCs, they exhibit poor electrical conductivity which limits their electrochemical performance [33]. The electrical conductivity of transition metal compounds can be enhanced by compositing them with carbon-based materials and conductive polymers [34–39,95]. To further improve the electrochemical performance (i.e., specific capacitance and cycling stability) of pseudocapacitors, researchers have focused on utilizing hollow nanoparticles as a potential material for supercapacitor electrodes [40]. This is due to their unique structure, which allows for a high surface area, efficient charge storage, and accommodation of volume expansion [30,40]. Studies have shown that hollow nanoparticles can lead to significantly improved performance of supercapacitors [32,40]. This has prompted researchers to explore various morphologies of transition metal compounds, such as hollow nanospheres [22,26,41,42], multi-shelled hollow micro- and nanospheres [13,43,44], and hollow nanocubes [31,35,45].

This review is essential as it consolidates recent advancements in the field of transition metal-based hollow micro- and nanoparticles for supercapacitor applications. By systematically analyzing the electrochemical performance of various transition metal compounds, including oxides, sulfides, phosphides/phosphates, and selenides, the review provides valuable insights into the potential of these materials. The emphasis on hollow structures and their impact on supercapacitor performance addresses a critical aspect of material design. This comprehensive overview not only informs researchers about the current state of the field but also identifies gaps and areas for further investigation, contributing to the advancement of high-performance supercapacitors.

2. Transition metal oxides (TMOs)

TMOs have attracted significant attention as a material for supercapacitor electrodes due to their high theoretical capacitance, low cost, and environmentally friendly properties [46]. The data presented in Table 1 illustrates the comparative electrochemical performance of various TMO-based hollow nanoparticles. In this study, we investigate the effect of various factors, including surface area, porosity, synthesis procedure, and morphologies on the electrochemical performance of the TMOs, with a specific focus on nickel, cobalt, and manganese oxides due to their superior electrochemical performance.

2.1. Nickel oxide

Nickel oxide (NiO) has garnered significant attention as a cost-effective and thermally stable electrode material for supercapacitors, owing to its thermal stability and theoretical specific capacitance of up to 2584 F g^{-1} [49]. The electrochemical performance of NiO as an electrode in supercapacitors is dependent on its surface morphological features such as surface area [49]. Reddy et al. [46] synthesized highly porous NiO hollow microspheres using metal-organic framework (MOF) which demonstrated improved electrical conductivity and ion transport channels for electrolytes compared to microflower structure, highlighting the importance of utilizing hollow morphology to enhance electrochemical performance [46]. The hollow microspheres exhibited a surface area of 38.54 m^2 g^{-1}, which was superior to the microflower structure (23.26 m^2 g^{-1}), further highlighting the significance of using hollow nanoparticles [46]. The resulting NiO material showed a specific capacitance of 1058 F g^{-1} which was higher than that of the microflower (857 F g^{-1}) [46]. In addition, the asymmetric supercapacitor (ASC) fabricated from NiO and Fe_2O_3 (noted as NiO||Fe_2O_3) displayed an energy density of 35.8 Wh kg^{-1} at a power density of 780 W kg^{-1} with over 93% capacity retention after 5000 cycles [46]. These results demonstrate the potential of NiO as a cost-effective and stable electrode material for supercapacitors where surface morphological features such as

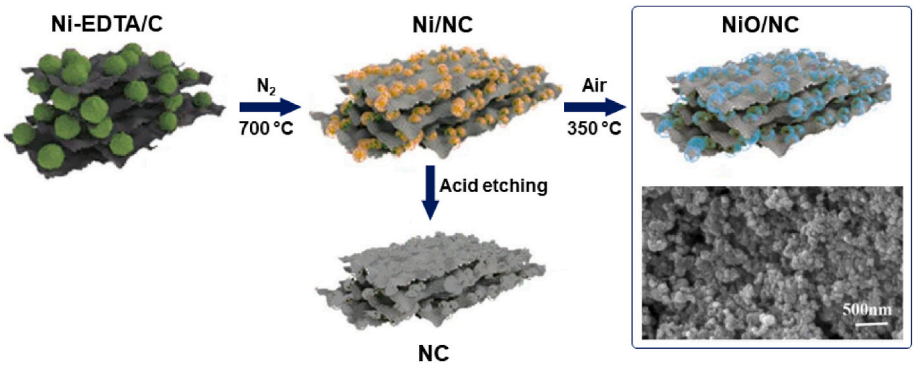

Fig. 1. Synthesis procedure of NiO/NC cathode in which the nickel ethylenediaminetetraacetate (Ni-EDTA) precursor undergoes pyrolysis under N_2 atmosphere and is subsequently oxidized in air, along with SEM image of NiO/NC. NC anode is prepared by acid etching the Ni/NC. Reprinted from reference [[29]], Copyright 2022, with permission from Elsevier [29].

surface area can greatly impact electrochemical performance.

NiO-based materials possess low conductivity which can lead to limitations in reaction kinetics and structural destruction [29]. To circumvent this issue, NiO can be embedded into the carbon matrix, as shown in Fig. 1 [29]. The incorporation of nanoparticles within a carbon matrix can improve the long-term cycling stability of the electrode materials as compared to a surface coating of the nanoparticles on a carbon substrate. This is attributed to the less separation between the nanoparticles and the carbon matrix [29]. Additionally, nitrogen-doping of carbon matrix (noted as NC) has been found to be effective in enhancing the capacitive behavior of carbon-based materials due to the ability of nitrogen dopants to alter the density of electronic states within the carbon skeleton, thereby enhancing the electron-accepting properties of adjacent nanoparticles [35]. It has been demonstrated in several studies, including the research conducted by Huang et al. [29], where hollow NiO nanoparticles embedded in nitrogen-doped carbon matrices (Fig. 1) resulted in a specific capacitance of 1026 F g^{-1} at 1 A g^{-1} [29]. Additionally, an ASC constructed from NiO/NC||NC exhibited a better cycle stability of 90.2% after 10000 cycles and achieved a higher energy density of 40.2 Wh kg^{-1} at a power density of 750.2 W kg^{-1} in comparison to previous study [29]. In summary, the research findings suggest that the electrochemical performance of NiO-based supercapacitors can be significantly improved by incorporating hollow nanoparticles and embedding them into a nitrogen-doped carbon matrix. These modifications have shown to increase energy density and cycling stability, indicating the potential for developing robust and efficient nickel-based electrode materials for energy storage applications.

2.2. Cobalt oxide

Cobalt oxide compounds, such as Co_3O_4, have gained interest as potential electrode materials for supercapacitors due to their high theoretical specific capacitance, superior thermal stability, and exceptional redox activity [50]. Despite these promising characteristics, there are still limitations that hinder their widespread application in supercapacitors [50]. One such limitation is the degradation of microstructure during charge-discharge cycles, leading to poor cycling stability [50]. To address this limitation, a promising approach is the synthesis of hollow multi-shelled structures (HoMSs) in which adjacent shells provide mutual support and improve cycling stability compared to single-shelled hollow nanoparticles [50]. Specifically, HoMSs are superior to single-shelled hollow structures in terms of utilizing the hollow space inside and maintaining a larger contact area between the electrode and electrolyte [50]. In this context, Wang et al. [50] synthesized precisely controlled single- (1 S-), double- (2 S-), triple- (3 S-), and quadruple- (4 S-) HoMSs of Co_3O_4 by a sequential templating approach. The 3 S-HoMSs were found to exhibit optimized charge storage capability and cycling stability [50]. This is attributed to the higher surface area of 3 S-HoMSs (22.9 m^2 g^{-1}) which surpasses that of 1 S-HoMSs (15.9 m^2 g^{-1}), 2 S-HoMSs (18.2 m^2 g^{-1}), and even 4 S-HoMSs (19.5 m^2 g^{-1}), likely due to thinner shell thickness in 3 S-HoMSs as depicted in Fig. 2 [50]. Additionally, 3 S-HoMSs displayed optimized specific capacitances of 688.2 F g^{-1} at a current density of 0.5 A g^{-1} with 93.2% cycling stability after 2000 cycles at 2.0 A g^{-1} [50].

Moreover, the incorporation of carbon-based materials has been shown to enhance the cycling stability of cobalt oxides by providing a carbonaceous framework that suppresses the agglomeration of nanoparticles, in addition to improving the electrical conductivity [51]. Liu et al. [51] deposited Co_3O_4 on the surface of *N*-doped carbon hollow nanospheres (NC@Co_3O_4) (Fig. 3A), which exhibited higher specific capacitance of 581.0 F g^{-1} at a current density of 1.0 A g^{-1} compared to Co_3O_4 nanorods (318.0 F g^{-1} at 1.0 A g^{-1}) [51]. While this performance is not superior to HoMSs-Co_3O_4, it showed an increased cycling stability (100% after 5000 cycles at 5.0 A g^{-1}) compared to the HoMSs-Co_3O_4 (93.2% after 2000 cycles at 2.0 A g^{-1}) [50,51]. In contrast to growing Co_3O_4, Yan et al. immobilized hollow Co_3O_4 within reduced graphene oxide (rGO)/carbon monolith (Co_3O_4/rGO/CM) (Fig. 3C) which resulted in higher specific capacitance of 1106.0 F g^{-1} at 1.0 A g^{-1} in

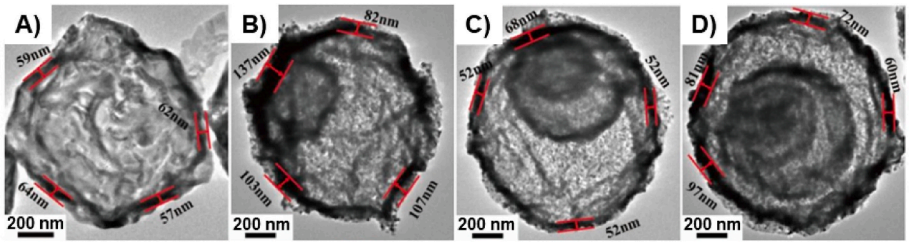

Fig. 2. TEM images of (A) 1 S-HoMSs (B) 2 S-HoMSs (C) 3 S-HoMSs (D) 4 S-HoMSs and their corresponding shell thicknesses. Thinner shell thickness can result in a higher surface area due to a better ion and electron transport to the surface of inner shells. Reprinted from reference [[50]], Copyright 2019, with permission from Springer Nature [50].

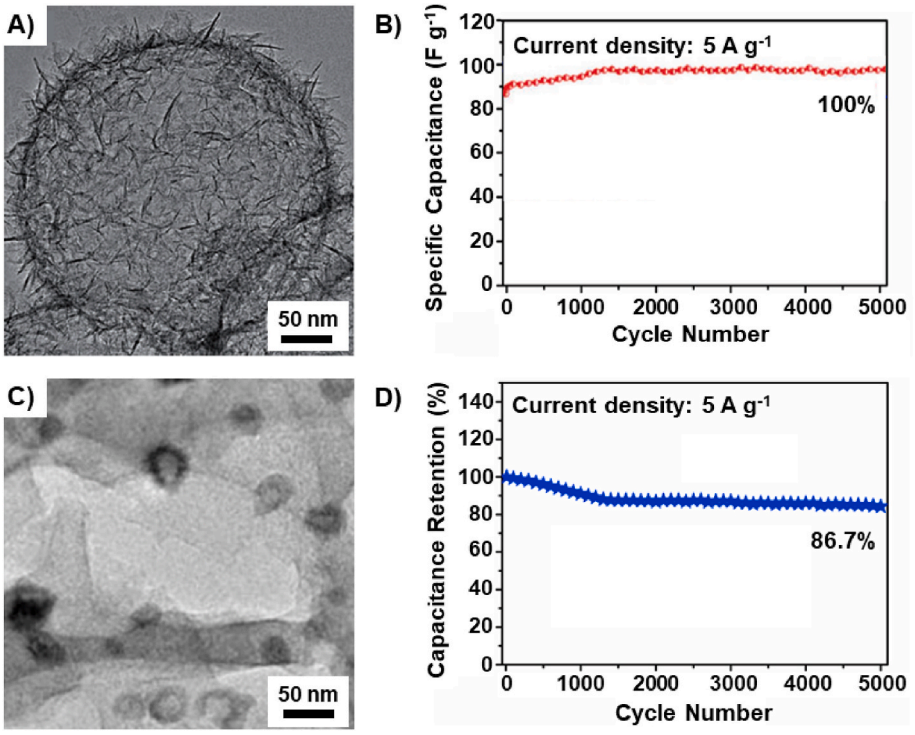

Fig. 3. (A) TEM image and (B) cycling stability of NC@Co_3O_4. Reprinted from reference [[51]], Copyright 2018, with permission from Wiley [51]. (C) TEM image and (D) cycling stability of Co_3O_4/rGO/CM. The growth of Co_3O_4 on carbon (NC@Co_3O_4) results in a higher cycling stability compared to embedding them in carbon (Co_3O_4/rGO/CM). Reprinted from reference [[52]], Copyright 2021, with permission from Elsevier [52].

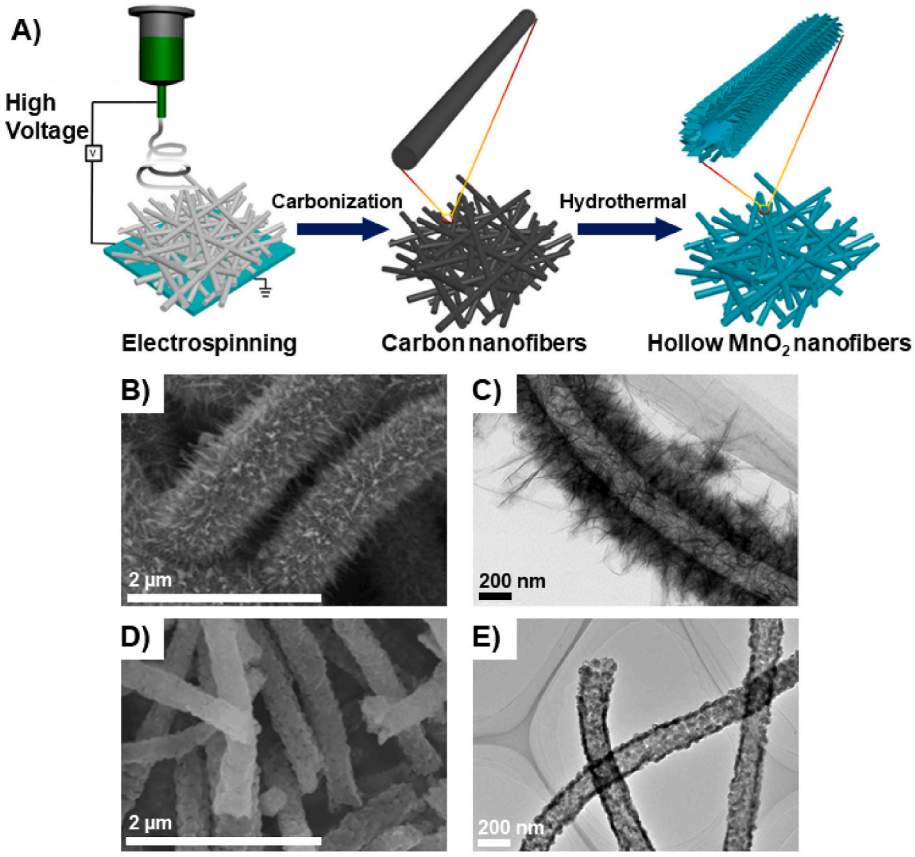

Fig. 4. (A) Schematic illustration of the electrospinning process used to create hollow MnO_2 nanofibers. Reprinted from reference [[40]], Copyright 2018, with permission from Elsevier [40]. (B) SEM and (C) TEM images of MnO_2 hollow nanofibers. (D) SEM and (E) TEM images of $ZnMn_2O_4$ hollow nanofibers. Reprinted from reference [[57]], Copyright 2021, with permission from Elsevier [57].

Table 2
Electrochemical and morphological comparison between TMS hollow nanoparticle-based supercapacitors.

Metal	Composition	Morphology	Specific Capacitance	Energy Density	Cycling Stability	Ref.
Cu	CuS	Hollow nanospheres	536.7 F g^{-1} at 8.0 A g^{-1}	16.0 Wh kg^{-1} at 185.4 W kg^{-1}	80.5% after 20000 cycles at 2.0 A g^{-1}	[65]
Mn	Mn_3O_4–MnS	Hollow multi-shelled microspheres	744.0 F g^{-1} at 1.0 A g^{-1}	65.8 Wh kg^{-1} at 800.0 W kg^{-1}	94.6% after 5000 cycles at 10.0 A g^{-1}	[44]
Ni	NiS_{1-x}@C	Hollow microspheres	1728.0 F g^{-1} at 1.0 A g^{-1}	36.9 Wh Kg^{-1} at 750.0 W kg^{-1}	75% after 5000 cycles at 50.0 mV s^{-1}	[66]
Co	$Co_{1-x}S$@NPSC	Hollow nanocubes	2206.0 F g^{-1} at 1.0 A g^{-1}	57.8 Wh kg^{-1} at 375.0 W kg^{-1}	83.2% after 8000 cycles at 5.0 A g^{-1}	[21]
Ni–Co	$NiCo_2S_4$	Hollow nanopolyhedra	1382.0 F g^{-1} at 1.0 A g^{-1}	35.3 Wh kg^{-1} at 750.0 W kg^{-1}	79% after 10000 cycles at 3.0 A g^{-1}	[64]
		Hollow nanoarrows	2161.7 F g^{-1} at 1.0 A g^{-1}	42.5 Wh kg^{-1} at 2684.2 W kg^{-1}	84.9% after 10000 cycles at 5.0 A g^{-1}	[67]
		Hollow microspheres	1688.0 F g^{-1} at 1.0 A g^{-1}	41.1 Wh kg^{-1} at 400.0 W kg^{-1}	62% after 10000 cycles at 5.0 A g^{-1}	[68]
		Hollow microspheres	1870.2 F g^{-1} at 2.0 A g^{-1}	52.9 Wh kg^{-1} at 374.9 W kg^{-1}	95.9% after 3000 cycles at 2.0 A g^{-1}	[69]
	$CoNi_2S_4$	Hollow nanocubes	2448.0 F g^{-1} at 1.0 A g^{-1}	62.2 Wh kg^{-1} at 775.0 W kg^{-1}	80.8% after 6000 cycles at 8.0 A g^{-1}	[70]
	$NiCo_2S_4$–Co_9S_8	Hollow nanospheres	2180.0 F g^{-1} at 1.0 A g^{-1}	96.5 Wh kg^{-1} at 800.0 W kg^{-1}	85% after 10000 cycles at 5.0 A g^{-1}	[71]
	C@$NiCo_2S_4$	Hollow nanospheres	1098.5 F g^{-1} at 0.5 A g^{-1}	35.1 Wh kg^{-1} at 203.5 W kg^{-1}	90% after 3000 cycles at 2.0 A g^{-1}	[72]
	C@$NiCo_2S_4$	Hollow nanospheres	1545.0 F g^{-1} at 2.0 A g^{-1}	34.1 Wh kg^{-1} at 160.0 W kg^{-1}	78.9% after 4000 cycles at 10.0 A g^{-1}	[26]
Ni–Co	$NiCo_2S_4$@C	Hollow nanoflake	1722.0 F g^{-1} at 1.0 A g^{-1}	38.3 Wh kg^{-1} at 800.0 W kg^{-1}	91.5% after 5000 cycles at 10.0 A g^{-1}	[73]
	Co_9S_8–Ni_3S_4	Hollow microspheres	1723.0 F g^{-1} at 1.0 A g^{-1}	49.5 Wh kg^{-1} at 760.0 W kg^{-1}	88.5% after 9000 cycles at 4.0 A g^{-1}	[61]
	Co_9S_8@$NiCo_2O_4$	Hollow nanoneedles	1022.5 F g^{-1} at 1.0 A g^{-1}	24.9 Wh kg^{-1} at 222 W kg^{-1}	88.9% after 6000 cycles at 8 A g^{-1}	[74]
Cu–Co	$CuCo_2S_4$@PANI	Hollow nanospheres	1120.0 F g^{-1} at 1.0 A g^{-1}	44.2 Wh kg^{-1} at 1000.0 W kg^{-1}	89.2% after 3000 cycles at 10.0 A g^{-1}	[75]
Zn–Co	$ZnCo_2S_4$	Hollow core-shell nanospheres	1045.3 F g^{-1} at 2.0 A g^{-1}	51.7 Wh kg^{-1} at 1700.0 W kg^{-1}	98.7% after 2000 cycles at 6.0 A g^{-1}	[76]
Mn–Co	$MnCo_2S_4$–$CoS_{1.097}$@C	Hollow double-shelled nanospheres	1006.0 F g^{-1} at 1.0 A g^{-1}	51.6 Wh kg^{-1} at 800.0 W kg^{-1}	87.9% after 10000 cycles at 5.0 A g^{-1}	[63]
V–Co	V_2O_5@Co_3S_4	Hollow core-shell nanowire	1493.6 F g^{-1} at 1.0 A g^{-1}	40.7 Wh kg^{-1} at 800.0 W kg^{-1}	85.9% after 10000 cycles at 10.0 A g^{-1}	[12]
Mn–Fe–Co	$MnFe_2O_4$@CoS_2	Hollow nanocubes	1490.0 F g^{-1} at 1.0 A g^{-1}	63.8 Wh kg^{-1} at 850.5 W kg^{-1}	88.5% after 10000 cycles at 12.0 A g^{-1}	[45]
Cu–Ni–Co	$Cu(NiCo)_2S_4$–Ni_3S_4	Hollow microflower	1320.0 F g^{-1} at 1.0 A g^{-1}	40.8 Wh kg^{-1} at 785.5 W kg^{-1}	85% after 5000 cycles at 15.0 A g^{-1}	[77]
Ni–Co–Mo	MoS_2–$NiCo_2S_4$@C	Hollow urchin-like microspheres	1800.0 F g^{-1} at 2.0 A g^{-1}	53.0 Wh kg^{-1} at 4200.0 W kg^{-1}	90.1% after 10000 cycles at 10.0 A g^{-1}	[62]
Ni–Co–Mn	NiCoMn–S	Hollow yolk-shell microspheres	1360.0 F g^{-1} at 1.0 A g^{-1}	49.8 Wh kg^{-1} at 1700.0 W kg^{-1}	98.2% after 6000 cycles at 10.0 A g^{-1}	[78]
		Hollow rod-like nanosheets	2098.2 F g^{-1} at 1.0 A g^{-1}	50.0 Wh kg^{-1} at 850.0 W kg^{-1}	73.6% after 6000 cycles at 10.0 A g^{-1}	[30]

comparison to NC@Co_3O_4 (581.0 F g^{-1} at 1.0 A g^{-1}) [51,52]. Also, Co_3O_4/rGO/CM||AC ASC showed a superior energy density (66.7 Wh kg^{-1} at 750.0 W kg^{-1}) compared to NC@Co_3O_4||AC (34.5 Wh kg^{-1} at 753.0 W kg^{-1}) [51,52]. However, the cycling stability of Co_3O_4/rGO/CM||AC (Figs. 3D and 86.7% after 5000 cycles at 5.0 A g^{-1}) was inferior to that of NC@Co_3O_4||AC (Figs. 3B and 100% after 5000 cycles at 5.0 A g^{-1}), indicating that the growth of Co_3O_4 on carbon materials (NC@Co_3O_4) may increase its cycling stability, as opposed to embedding them (Co_3O_4/rGO/CM) [51,52].

In order to attain the full theoretical specific capacitance of 3560 F g^{-1} for cobalt oxide compounds, the integration of conductive polymers, such as polyaniline (PANI), can be an effective approach [34]. Ren et al. synthesized hollow Co_3O_4@PANI nanocages using a facile self-sacrificing template method in combination with in-situ polymerization [34]. While the Co_3O_4@PANI nanocages showed improved specific capacitance (1301.0 F g^{-1} at 1.0 A g^{-1}) and energy density (41.5 Wh kg^{-1} at 800.0 W kg^{-1}) compared to NC@Co_3O_4 (581.0 F g^{-1} at 1.0 A g^{-1} and 34.5 Wh kg^{-1} at 753.0 W kg^{-1}), it exhibited lower cycling stability of 83.4% after 5000 cycles at 5.0 A g^{-1} in comparison with carbon-integrated electrodes [34,51]. This can be attributed to the lack of structural support provided by polymer-integrated electrodes [34,51]. Another effective approach to enhance specific capacitance is through the utilization of binary metal oxides [22]. They offer a range of oxidation states and synergistic interactions between the metal oxides, resulting in increased electrical conductivity and improved redox activity [22]. Studies have been performed investigating the use of bimetal oxides, including $NiCo_2O_4$ [35], $Co_3V_2O_8$ [22], $ZnCo_2O_4$ [53], $CuCo_2O_4$ [55], and $CoMn_2O_4$ [58] as potential electrode materials for supercapacitors. In particular, $Co_3V_2O_8$, a low-cost mixed transition metal oxide, has been demonstrated to possess a high specific capacitance [22]. The strong binding strength between vanadium and oxygen prevents the vanadium from reaching a zero oxidation state (metallic vanadium) during charge/discharge processes, leading to relatively low volume changes compared to other metal oxides [22]. These hollow $Co_3V_2O_8$ nanospheres were synthesized via a facile hydrothermal method [22]. The synthesized nanoparticles exhibited high specific capacitance and cycling stability. In the same study, the $Co_3V_2O_8$||AC ASC was also fabricated, which demonstrated high energy density of 59.2 Wh kg^{-1} at the power density of 250.0 W kg^{-1}. Then, incorporating other transition metals into the cobalt oxide-based supercapacitors can enhance their electrochemical performance such as specific capacitance. For instance, $Co_3V_2O_8$ exhibits a specific capacitance of 2376.0 F g^{-1} at

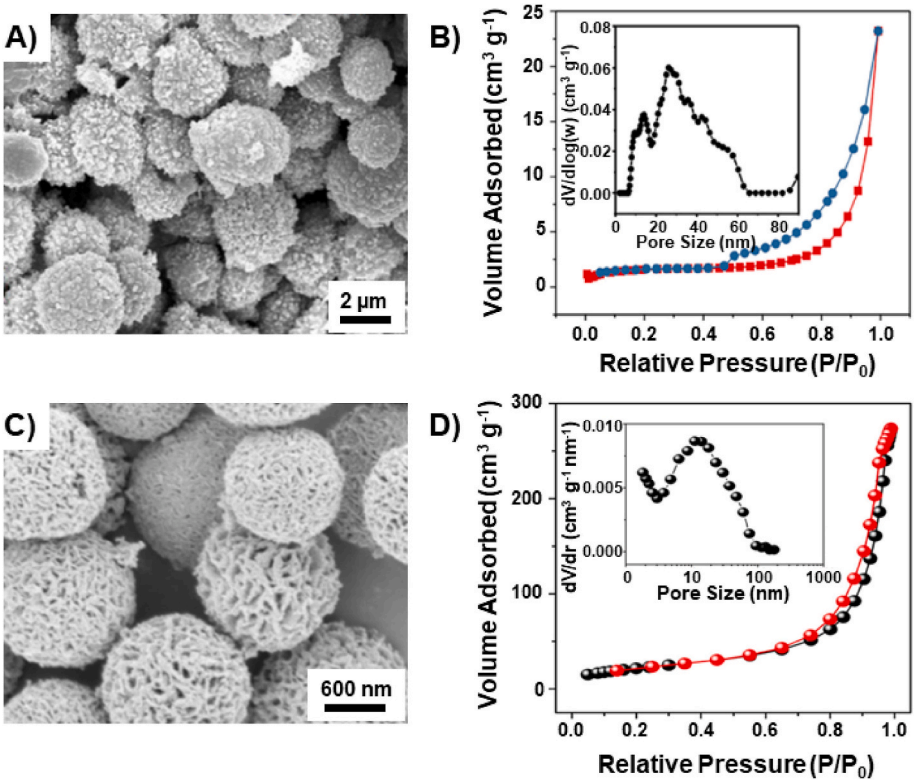

Fig. 5. (A) SEM image and (B) nitrogen adsorption-desorption isotherm (inset is the pore size distribution) of waxberry-like $NiCo_2S_4$. Reprinted from reference [[68]], Copyright 2020, with permission from Elsevier [68]. (C) SEM image and (D) nitrogen adsorption-desorption isotherm (inset is the pore size distribution) of highly porous $NiCo_2S_4$. Reprinted from reference [[69]], Copyright 2018, with permission from Elsevier [69].

2.0 A g^{-1}, which is significantly higher than that of Co3O4, which only exhibits a specific capacitance of 688.2 F g^{-1} at 0.5 A g^{-1}.

2.3. Manganese dioxide

Manganese dioxide (MnO_2) is a cost-effective and environmentally friendly alternative as an electrode material for supercapacitors due to its high theoretical specific capacitance and stability [40,59]. However, the poor electrical conductivity and low reaction kinetics of MnO_2 as a single metal oxide, limit its practical application in supercapacitors [40]. To address these limitations, various strategies have been proposed, such as manipulating the morphological properties of MnO_2 nanostructures [40,44,60]. One such strategy is the development of hollow MnO_2 nanofibers, as a 1D nanostructure, which provides high specific capacitance due to having a short distance for ion and electron transport [40]. Xu et al. developed hollow MnO_2 nanofibers using facile electrospinning of carbon nanofibers (Fig. 4A–C), served as a sacrificial template, and achieved a specific capacitance of 291.0 F g^{-1} at a current density of 1.0 A g^{-1} [40]. Additionally, the specific capacitance of Mn-based SCs can be further improved by synthesizing spinel zinc-manganese oxide ($ZnMn_2O_4$) nanofibers (Fig. 4D and E) [57]. The multiple oxidation states of $ZnMn_2O_4$ lead to enhance electrochemical performance compared to single-component TMOs [57]. Yun et al. synthesized $ZnMn_2O_4$ nanofibers with a higher specific capacitance (1026.0 F g^{-1} at 2.0 A g^{-1}) and superior capacitance retention (100.8% after 5000 cycles at 6.0 A g^{-1}) in comparison with the MnO_2 nanofibers (291.0 F g^{-1} at 1.0 A g^{-1}, 90.9% after 5000 cycles at 50 mV s^{-1}) [57].

3. Transition metal sulfides (TMSs)

TMSs have emerged as highly promising electrode materials for supercapacitors due to their high theoretical capacitance, high conductivity, high redox activity, low cost, and long lifespan [61–63]. TMSs exhibit superior electrical conductivity compared to their oxide counterparts due to sulfur's relatively lower electronegativity, which facilitates the ease of electron transport. This increased conductivity is beneficial in achieving high specific capacitance [64]. Herein, we explore the factors that impact the electrochemical performance of TMS-based hollow nanoparticles (Table 2). The primary focus of this investigation is on the effects of varying conditions on the electrochemical performance of the nickel-cobalt sulfide-based and nickel-cobalt-manganese sulfide-based hollow nanoparticles.

3.1. Nickel–cobalt sulfide

Bimetallic sulfides, such as nickel-cobalt sulfide ($NiCo_2S_4$ and $CoNi_2S_4$), have exhibited superior electrochemical performance compared to monometallic sulfides due to the cooperative contribution of two different ions that provide alterable valences [68]. Furthermore, the narrow band gap of nickel-cobalt sulfide can accelerate charge/discharge processes and makes it a promising electrode material with high electrical conductivity [68]. Gao et al. synthesized waxberry-like $NiCo_2S_4$ hollow microspheres (Fig. 5A) which exhibited an average pore size of 30 nm as determined by nitrogen adsorption-desorption isotherm (Fig. 5B) [68]. The waxberry-like $NiCo_2S_4$ nanoparticles exhibited a specific capacitance of 1688.0 F g^{-1} at a current density of 1.0 A g^{-1} [68]. The ASC composed of $NiCo_2S_4$ on an active rice husk carbon (ARHC) (noted as $NiCo_2S_4$|| ARHC) showed an energy density of 41.1 Wh kg^{-1} at a power density of 400.0 W kg^{-1}, and a cycling stability of 62% after 10000 cycles (~76% after 3000 cycles) at 5.0 A g^{-1} [68]. In another study, Wei et al. synthesized highly porous $NiCo_2S_4$ hollow microspheres (Fig. 5C) with an average pore size of 12 nm (Fig. 5D) [69]. Despite the smaller average pore size in comparison to the previous study, the increased surface porosity and larger surface area led to a higher specific capacitance of 1870.2 F g^{-1} at a current density of 2.0 A g^{-1} and a superior energy density of 52.9 Wh kg^{-1} at 374.9 W kg^{-1} [69].

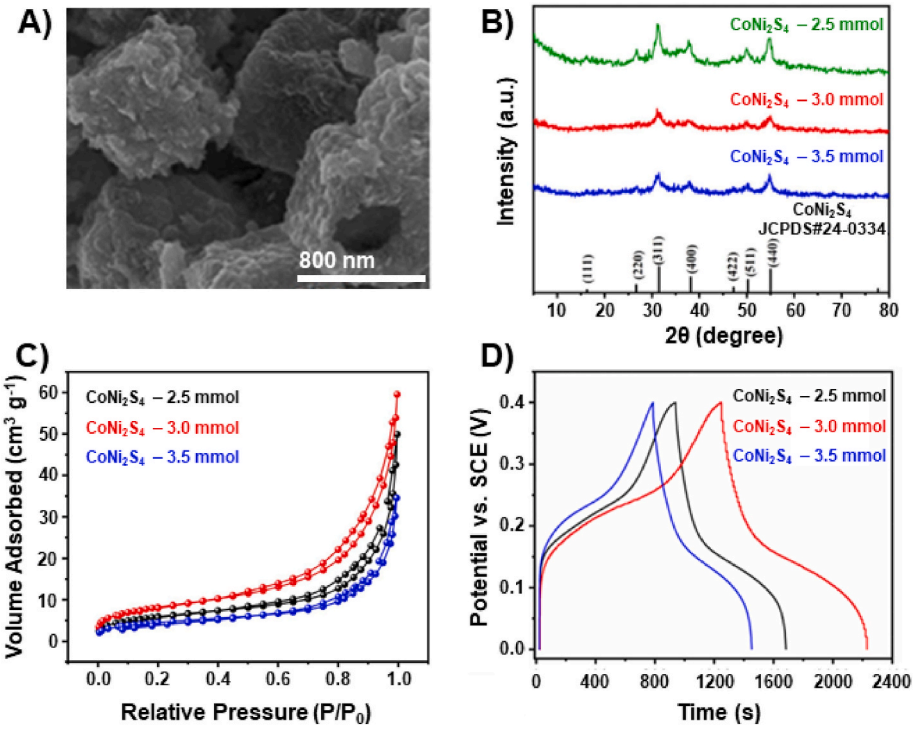

Fig. 6. (A) SEM image of the $CoNi_2S_4$ hollow nanocubes with a sulfur content of 3 mmol, (B) XRD pattern, (C) nitrogen adsorption-desorption isotherm, and (D) GCD curves at a current density of 1 A g^{-1} for $CoNi_2S_4$ with varying sulfur content. Reprinted from reference [[70], Copyright 2021, with permission from Elsevier [70].

Also, the cycling stability improved to 95.9% after 3000 cycles at 2.0 A g^{-1} compared to the previous study [69]. The mesoporous structure of nanoparticles studied here highlights the importance of porosity in determining the electrochemical performance of $NiCo_2S_4$-based materials, as increasing the porosity and creating highly porous structures can provide more channels for ion and electron diffusion, thus facilitating access to the electrode materials and resulting in an increase in specific capacitance [64,68,69].

The electrochemical performance of nickel-cobalt sulfide materials can be enhanced by the manipulation of sulfur content in nanoparticles with the aim of reducing crystallinity [15,70]. High degree of crystallinity can lead to a tightly packed structure and result in reduced porosity and lower electrochemical performance [49]. The relation between sulfur content and crystallinity can be assessed through analysis of the diffraction peaks in X-ray diffraction (XRD) pattern where a weaker XRD peak indicates lower crystallinity [70]. Chen et al. synthesized $CoNi_2S_4$ hollow nanocubes (Fig. 6A) with different sulfur content (2.5 mmol, 3.0 mmol, and 3.5 mmol) and optimized their specific capacitance by reducing the crystallinity through manipulation of the sulfur content in the nanoparticles (Fig. 6B) [70]. This resulted in a maximum active surface area for the sample with 3 mmol of sulfur (Fig. 6C) which exhibited the highest specific capacitance of 2448.0 F g^{-1} at a current density of 1.0 A g^{-1}, as determined by galvanostatic charge-discharge (GCD) measurements (Fig. 6D) [70]. Also, the calcination temperature has been shown to play a crucial role in the final performance of the electrode, as it can affect the crystallinity of the material [70,71]. Han et al. demonstrated that an optimized calcination temperature for Ni–Co hydroxide can improve the electrochemical performance of the resulting $NiCo_2S_4$–Co_9S_8 hollow nanospheres [71]. It is worth noting that the energy density of the $NiCo_2S_4$–Co_9S_8 nanoparticles was particularly high, reaching 96.5 Wh kg^{-1} at a power density of 800.0 W kg^{-1}, in addition to achieving a specific capacitance of 2180.0 F g^{-1} at 1.0 A g^{-1} [71].

The poor cycle stability of Ni–Co sulfide electrodes is primarily attributed to structural degradation, as well as the susceptibility of the $NiCo_2S_4$ electrodes to oxidation in alkaline electrolytes, leading to a rapid decline in electrical conductivity during prolonged cycling operations [26,66,72,73]. To address this issue, the hybridization of Ni–Co sulfides with carbon materials can be utilized [26,72,73]. The addition of carbonaceous materials not only improves the conductivity of the composite electrode but also acts as a matrix to support the growth of $NiCo_2S_4$ and inhibit the agglomeration of $NiCo_2S_4$ nanoparticles, thus promoting the long-term stability of the electrode [26]. It is noteworthy that the method of incorporating carbon into the $NiCo_2S_4$, such as adding carbon to the $NiCo_2S_4$ versus growing $NiCo_2S_4$ on a carbon shell, may have an impact on the electrochemical performance of the resulting materials [26,72,73]. In a study by Mohamed et al., the incorporation of carbon into mesoporous $NiCo_2S_4$ hollow nanoflakes led to an improved cycling stability of 91.5% after 5000 cycles at 10.0 A g^{-1} and higher specific capacitance of 1722.0 F g^{-1} at 1.0 A g^{-1} compared to a study by Liu et al., in which microporous $NiCo_2S_4$ was grown on a carbon shell (C@$NiCo_2S_4$) resulting in a specific capacitance of 1098.5 F g^{-1} at 0.5 A g^{-1} and cycling stability of 90% after 3000 cycles at 2.0 A g^{-1} [72,73]. The improved performance in the case of carbon-containing $NiCo_2S_4$ hollow nanoflakes may be attributed to the addition of carbon to the $NiCo_2S_4$ and resulting a mesoporous structure, which provides more channels for ion and electron diffusion, led to increasing the specific capacitance and cycling stability [26,72,73].

3.2. *Nickel–cobalt–manganese sulfide*

Ternary hybrid metal sulfides, which comprise three metal elements, have been found to exhibit superior electrochemical performance as electrodes in supercapacitors compared to binary metal sulfides [30,78]. This is attributed to the presence of a stronger synergistic effect, a greater number of mixed-valence states, and a higher density of redox-active centers, which are characteristic of the ternary systems [30,78]. Among the hybrid metal sulfides, Ni–Co based materials have been identified as particularly promising for high-performance electrochemical energy storage [26,64,67–73]. The inclusion of p-type semiconductors, such as MnS, which possess high theoretical capacitance and good conductivity, has been shown to enhance the performance of

Table 3
Electrochemical and morphological comparison between TMP hollow nanoparticle-based supercapacitors.

Metal	Composition	Morphology	Specific Capacitance	Energy Density	Cycling Stability	Ref.
Fe	FeP/PGNPC	Hollow nanospheres	696.0 F g^{-1} at 1.0 A g^{-1}	112.0 Wh kg^{-1} at 850.0 W kg^{-1}	90% after 5000 cycles at 10.0 A g^{-1}	[47]
Ni	NiP	Hollow microspheres	1625.0 F g^{-1} at 1.0 A g^{-1}	—	65% after 10000 cycles at 10.0 A g^{-1}	[81]
	Ni_2P/C	Hollow microspheres	1676.0 F g^{-1} at 1.0 A g^{-1}	42.7 Wh kg^{-1} at 764.2 W kg^{-1}	95% after 5000 cycles at 10.0 A g^{-1}	[82]
Co	CoP	Hollow pompon-like microspheres	449.4 F g^{-1} at 1.0 A g^{-1}	22.2 Wh kg^{-1} at 374.9 W kg^{-1}	80.9% after 3000 cycles at 2.0 A g^{-1}	[83]
		Hollow microcubes	560.0 F g^{-1} at 1.0 A g^{-1}	21.4 Wh kg^{-1} at 373.0 W kg^{-1}	81.2% after 6000 cycles at 1.0 A g^{-1}	[84]
Ni–Co	NiCoP	Hollow nanopolyhedra	1616.0 F g^{-1} at 1.0 A g^{-1}	33.3 Wh kg^{-1} at 150.0 W kg^{-1}	67.2% after 10000 cycles at 1.0 A g^{-1}	[80]
	NiCoP	Hollow microcubes	1258.0 F g^{-1} at 1.0 A g^{-1}	43.2 Wh kg^{-1} at 801.6 W kg^{-1}	90.1% after 10000 cycles at 4.0 A g^{-1}	[79]
	NiCoP–C	Hollow nanospheres	2599.8 F g^{-1} at 1.0 A g^{-1}	54.7 Wh kg^{-1} at 794.7 W kg^{-1}	90.6% after 10000 cycles at 20.0 A g^{-1}	[85]
	NiCoP@NC	Hollow nanocubes	1127.0 F g^{-1} at 1.0 A g^{-1}	52.5 Wh kg^{-1} at 750.2 W kg^{-1}	83.2% after 6000 cycles at 40.0 mV s^{-1}	[86]
	NiCoP-NPC	Hollow nanospheres	1200.5 F g^{-1} at 1.0 A g^{-1}	40.2 Wh kg^{-1} at 800.2 W kg^{-1}	81.8% after 5000 cycles at 4.0 A g^{-1}	[87]
	NiCo–P/S@CNT/rGO	Hollow nanospheres	1552.4 F g^{-1} at 1.0 A g^{-1}	33.2 Wh kg^{-1} at 800.0 W kg^{-1}	87.1% after 1000 cycles at 3.0 A g^{-1}	[16]
	NiCoP/PrGO	Hollow microspheres	2586.9 F g^{-1} at 1.0 A g^{-1}	49.7 Wh kg^{-1} at 366.0 W kg^{-1}	99% after 5000 cycles at 30.0 A g^{-1}	[88]
Cu–Ni	CuNiP/rGO	Hollow nanospheres	2150.0 F g^{-1} at 1.0 A g^{-1}	64.0 Wh kg^{-1} at 801.0 W kg^{-1}	91.8% after 13000 cycles at 15.0 A g^{-1}	[89]
Mn–Co	MnCoP	Hollow nanocubes	2197.5 F g^{-1} at 2.0 A g^{-1}	67.0 Wh kg^{-1} at 2550.0 W kg^{-1}	93.7% after 6000 cycles at 36.0 mA cm^{-2}	[31]

TMS materials [78]. However, the aggregation of MnS nanoparticles during redox reactions remains a significant challenge that limits its practical application [78]. By incorporating MnS into Ni–Co sulfide composites, not only can this issue be addressed, but it also increases the available electrode-electrolyte interface area for charge transfer reactions, thereby improving overall electrochemical performance [78]. Wei et al. synthesized yolk-shell structured Ni–Co–Mn sulfide nanoparticles through a solvothermal preparation method [78]. The unique structure of these particles resulted in a specific capacitance of 1360.0 F g^{-1} at a current density of 1 A g^{-1} and an energy density of 49.8 Wh kg^{-1} at a power density of 1700.0 W kg^{-1} [78]. The yolk-shell structure of these particles was found to effectively accommodate volume expansion and reduce the diffusion path for electrolyte ions [78]. The synergistic effect of the rational composition of Ni–Co–Mn sulfide leads to an improvement in the electrochemical performance of supercapacitors [78]. Kang et al. demonstrated the effect of different Ni/Co/Mn ratios on the electrochemical performance of trimetallic sulfides through the synthesis of samples by utilizing MOFs [30]. The results

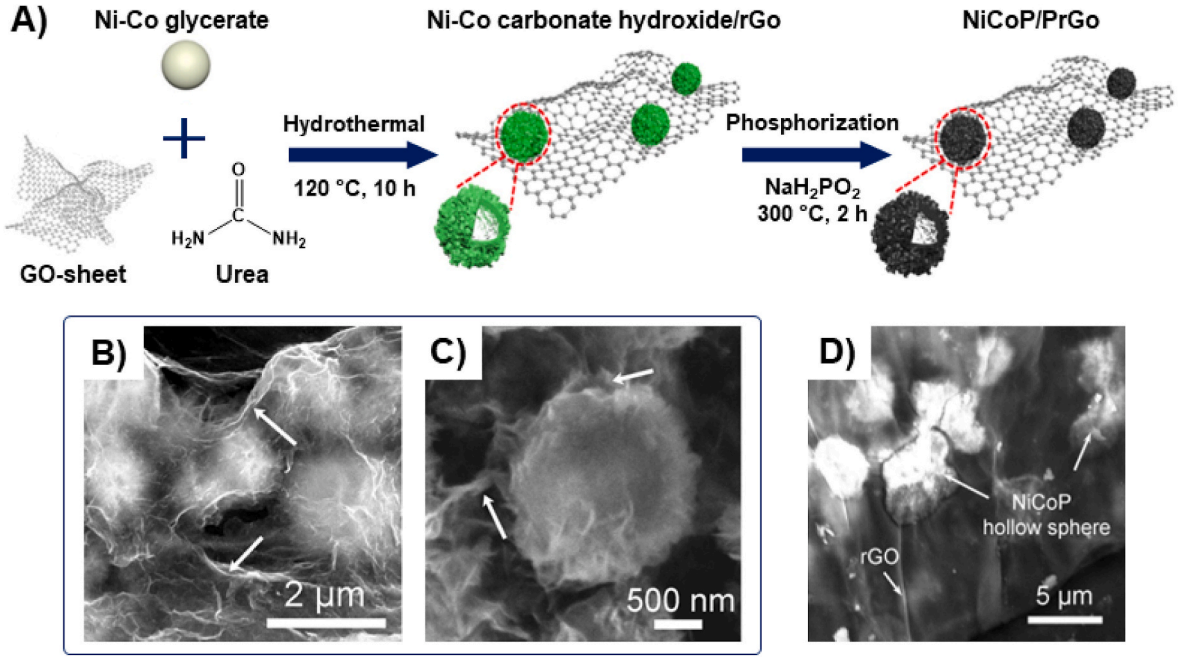

Fig. 7. (A) Synthesis procedure of NiCoP/PrGO, (B,C) SEM images of NiCoP/PrGO (arrows show the tightly-wrapped NiCoP hollow microspheres in PrGO), and (D) SEM image of NiCoP/rGO (arrows show the separation between NiCoP hollow microspheres and rGO). Reprinted from reference [[88]], Copyright 2019, with permission from Elsevier [88].

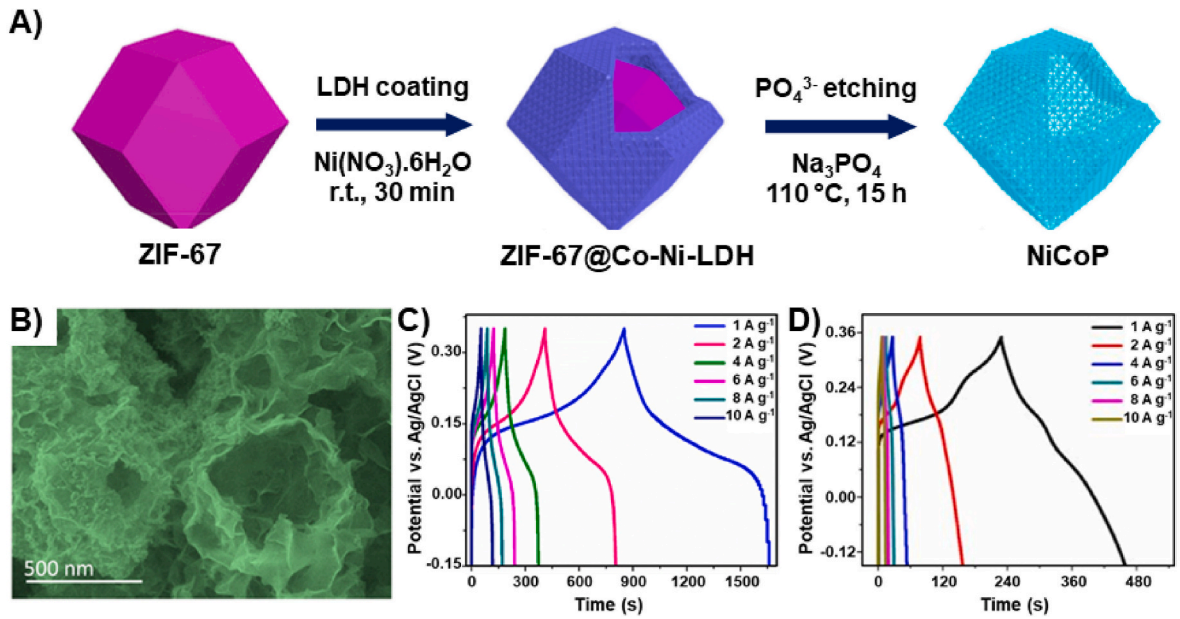

Fig. 8. (A) Schematic illustration of the synthesis route of Ni–Co phosphate hollow nanopolyhedra (B) SEM image of NiCoP (C,D) GCD measurements of NiCoP and ZIF-67@Co–Ni-LDH, respectively. Reprinted from reference [[80]], Copyright 2019, with permission from American Chemical Society [80].

indicated that the electrochemical properties of the samples were dependent on their composition and the optimized ratio of Ni/Co/Mn in trimetallic sulfides (NiCoMn–S) has been shown to result in superior electrochemical performance, owing to the maximum synergistic effect of the transition metal ions present [30,68]. The NiCoMn–S samples exhibited a specific capacitance of 2098.2 F g^{-1} at a current density of 1.0 A $^{-1}$, and an energy density of 50.0 Wh kg^{-1} at a power density of 850.0 W kg^{-1} [30]. Notwithstanding, the ternary metal sulfide-based supercapacitors are still in their nascent stage of development and their cycling stability and energy density have not surpassed those of nickel-cobalt sulfide-based supercapacitors.

4. Transition metal phosphides/phosphates (TMPs)

TMPs are a class of n-type semiconductor materials that exhibit metal-like properties and ultra-fast electron conductivity, outperforming transition metal oxides and hydroxides in terms of electrical conductivity and electrochemical properties [79]. The transition metal phosphides/phosphates possess several advantages including high theoretical capacitance, natural abundance, and environmentally friendly nature [79–81]. Despite their numerous advantages, researchers continue to explore different ways to optimize the electrochemical activity and cycle stability of TMPs, working towards realizing their full potential as a top-performing supercapacitor material. In this section, we will investigate the unique characteristics of phosphides/phosphates-based micro- and nanoparticles (Table 3) and highlight their potential as a valuable material in this field.

4.1. Nickel–cobalt Phosphide/phosphate

The development of high-performance electrode materials has led to the investigation of various metal phosphides/phosphates, with Ni- and Co-based phosphides/phosphates emerging as promising candidates [79]. Ni-based phosphides/phosphates possess high theoretical capacitance but show limitations in terms of cycling stability [79,81]. On the other hand, Co-based phosphides/phosphates exhibit excellent capacitance rate and cycling stability during charging and discharging cycles, making them an attractive choice for high-performance electrode materials [79,80]. As a result, the construction of cobalt-nickel bimetallic phosphides/phosphates is considered a valuable strategy in the pursuit of advanced electrode materials [79]. Zhang et al. synthesized NiCoP hollow microcubes with varying ratios of nickel to cobalt starting materials (Ni:Co of 1:0, 2:1, 1:1, 1:2, and 0:1) to investigate the impact of the ratio on the final electrochemical performance [79]. Results showed that the hollow microcubes with a 2:1 Ni:Co ratio exhibited the highest specific capacitance of 629.0 C g^{-1} (1258.0 F g^{-1}) at 1.0 A g^{-1} [79].

The electrochemical performance of TMPs can be improved through the incorporation of carbon-based materials [85]. Several studies have demonstrated the utilization of different types of carbon, such as carbon nanoparticles, *N*-doped carbon [86], *N*,P-doped carbon [87], carbon nanotubes/reduced graphene oxide (CNT/rGO) [16], and P-doped reduced graphene oxide (PrGO) [88], can enhance the electrochemical performance of TMPs [88]. Dong et al. synthesized NiCoP/P-doped rGO (NiCoP/PrGO) hollow microspheres through a hydrothermal treatment of a mixture of NiCo-based microspheres in graphene oxide (GO) suspension followed by a phosphorization process as it is illustrated in Fig. 7A [88]. It is noteworthy that the carbonaceous matrix envelops the particles in the NiCoP/PrGO sample (Fig. 7B and C), while the NiCoP/rGO sample which was directly prepared from hollow NiCoP and rGO does not exhibit an interconnected network (Fig. 7D) [88]. This highlights the importance of the hydrothermal process in the preparation of the mixture of NiCo and GO sheets [88]. The NiCoP/PrGO hollow microspheres exhibit an improved specific capacitance (2586.9 F g^{-1} at 1.0 A g^{-1}) compared to other TMPs not incorporating carbon-based materials [88].

Ni–Co phosphates have an open framework structure that provides larger cavities and more active sites, resulting in higher ion/charge conductivity compared to the tightly packed molecular structure of Ni–Co phosphides [80]. Additionally, the presence of P–O bonds in phosphates provides more stable redox couples [80,81]. However, the synthesis of hollow bimetallic phosphates remains challenging due to limited control over the synthesis process [80]. Xiao et al. synthesized Ni–Co phosphates hollow nanopolyhedra through the coating of a specific type of MOFs (ZIF-67) with nickel-cobalt layered double hydroxides (ZIF-67@Co–Ni-LDHs) followed by controllable etching of ZIF-67@Co–Ni-LDHs (Fig. 8A and B) [80]. The etching process with Na_3PO_4 was shown to enhance the electrochemical performance of the Ni–Co phosphates compared to the LDH precursor as it is shown in Fig. 8C and D [80]. The Ni–Co phosphates nanopolyhedra displayed a high specific capacitance of 1616.0 F g^{-1} at 1.0 A g^{-1} (Fig. 8C), which was

Table 4
Electrochemical and morphological comparison between TMSe hollow nanoparticle-based supercapacitors.

Metal	Composition	Morphology	Specific Capacitance	Energy Density	Cycling Stability	Ref.
Ni–Co	$NiSe_2$–$CoSe_2$	Hollow microspheres	1234.8 F g^{-1} at 1.0 A g^{-1}	53.7 Wh kg^{-1} at 130.2 W kg^{-1}	92.2% after 5000 cycles at 10.0 A g^{-1}	[90]
Ni–Mn	Ni–Mn–Se	Hollow multi-shelled microspheres	2035.2 F g^{-1} at 2.0 A g^{-1}	112.6 Wh kg^{-1} at 900.8 W kg^{-1}	96.1% after 10000 cycles at 32.0 A g^{-1}	[13]
Ni–Fe	Ni–Fe–Se	Hollow double-shelled microspheres	775.2 F g^{-1} at 2.0 A g^{-1}			
Cu–Co	Cu–Co–Se	Hollow microspheres	1124.0 F g^{-1} at 2.0 A g^{-1}	32.4 Wh kg^{-1} at 800.0 W kg^{-1}	93.7% after 5000 cycles at 10.0 A g^{-1}	[91]
Co–Mo	Co–Mo–Se	Hollow double-shelled nanopolyhedra	1320.3 F g^{-1} at 2.0 A g^{-1}	45.0 Wh kg^{-1} at 2222.0 W kg^{-1}	94% after 8000 cycles at 17.0 mA cm^{-2}	[92]
Co–Mo	$CoSe_2$–$MoSe_2$	Hollow nanospheres	1907.7 F g^{-1} at 1.0 A g^{-1}	51.8 Wh kg^{-1} at 799.2 W kg^{-1}	93.4% after 10000 cycles at 5.0 A g^{-1}	[41]
Zn–Co	Zn–Co–Se/rGO	Hollow multi-shelled nanospheres	2260.5 F g^{-1} at 2.0 A g^{-1}	126.3 Wh kg^{-1} at 902.2 W kg^{-1}	91.7% after 12000 cycles at 32.0 A g^{-1}	[93]
Co–Fe	Co–Fe–Se/rGO	Hollow yolk-double-shelled nanospheres	879.3 F g^{-1} at 2.0 A g^{-1}			

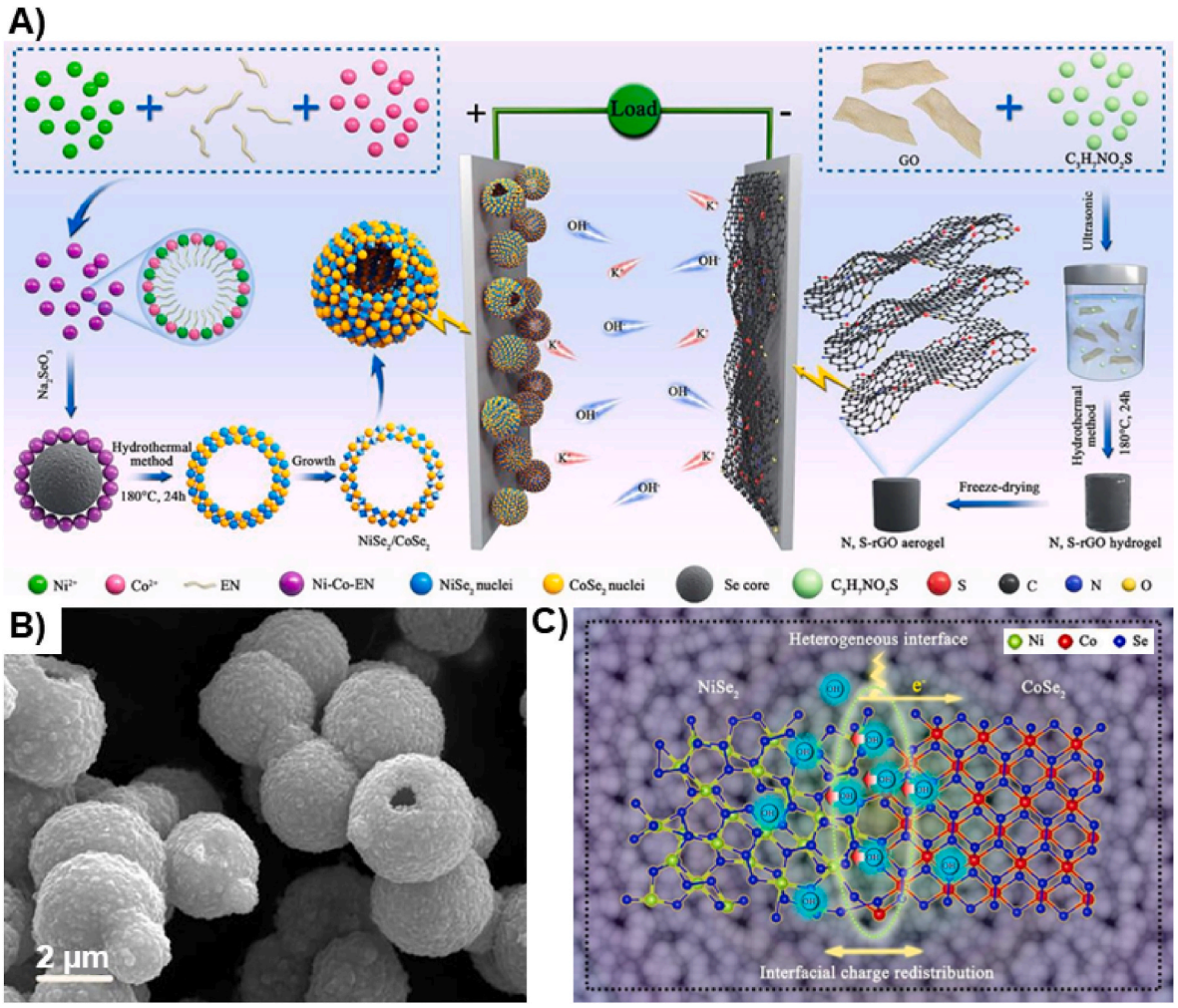

Fig. 9. (A) Schematic illustration of the synthesis processes of $NiSe_2/CoSe_2$ cathode, *N*,S-rGO aerogel anode, and $NiSe_2/CoSe_2$||N,S-rGO ASC. (B) SEM image of the heterostructured $NiSe_2/CoSe_2$ hollow microspheres. (C) Schematic representation of the phase-boundary effect in heterostructured $NiSe_2/CoSe_2$. Reprinted from reference [[90]], Copyright 2021, with permission from Elsevier [90].

significantly higher than that of the LDH precursor (Figs. 8D and 460.0 F g^{-1} at 1.0 A g^{-1}) and even higher than the Ni–Co phosphides [79] (1258.0 F g^{-1}), demonstrating the potential improvement attainable through the utilization of phosphates [80].

5. Transition metal selenides (TMSes)

Descending the 16th column of the periodic table, TMSes have exhibited distinctive characteristics such as lower bandgap, higher concentration of redox sites, and enhanced conductivity in comparison to TMOs and TMSs [90]. Selenide possesses a lower electronegativity and exhibits a significantly higher conductivity (1×10^{-3} S m^{-1}) compared to that of oxygen (1×10^{-5} S m^{-1}) and sulfur (1×10^{-28} S m^{-1}) [41]. However, the practical application of TMSe is limited by its low cycling stability resulting from its substantial volume expansion [41]. To address this challenge, the synthesis of hollow TMSe nanoparticles has been proposed as a potential solution [41]. Despite the limited research conducted on the TMSe hollow nanoparticles, recent advances in the field have indicated their potential for being utilized in the TMSe-based supercapacitor. In this study, we aim to review the

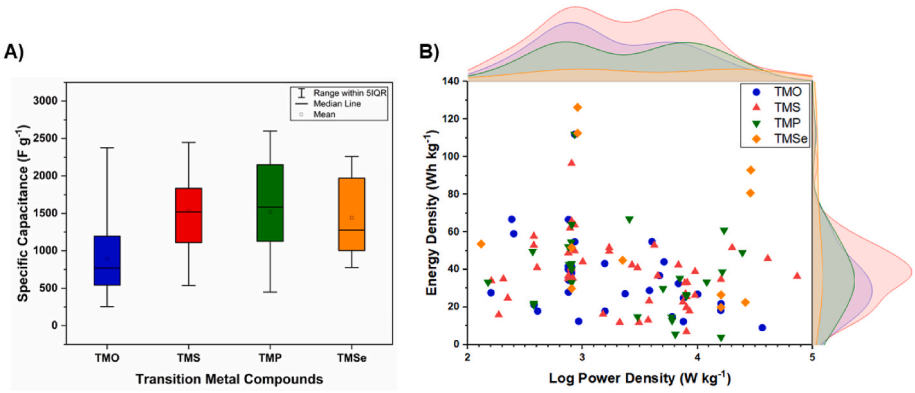

Fig. 10. (A) Comparison of the specific capacitance between the hollow micro- and nanoparticles studied in this review. (B) Ragone plot of the transition metal-based micro- and nanoparticles explored in this review (the intensities displayed on the distribution curves represent the quantity of data corresponding to each axis).

recent progress made in the electrochemical performance of the hollow TMSe-based micro- and nanoparticles (Table 4).

5.1. Nickel selenide

Nickel-based selenides possess favorable electrochemical properties, attributed to the high redox activity of nickel. The electrochemical properties of Ni-based selenides can be enhanced through the development of heterostructures. The presence of phase boundaries within these heterostructures often leads to an increase in lattice defects and distortions, thereby enhancing interfacial charge transfer and accelerating electrochemical kinetics. Furthermore, synergistic effects derived from the chemical bonding of different metal ions are expected to further enhance the electrochemical properties. Yun et al. synthesized heterostructured $NiSe_2/CoSe_2$ hollow microspheres through a one-pot hydrothermal method involving Se@Ni–Co-ethylenediamine (Se@Ni–Co-EN) core-shell, as illustrated in Fig. 9A. The heterostructured $NiSe_2/CoSe_2$ hollow microspheres (Fig. 9B) exhibited higher specific capacitance (1234.8 F g^{-1} at 1.0 A g^{-1}) compared to the hollow $NiSe_2$ microspheres (1045.4 F g^{-1} at 1.0 A g^{-1}) and the hollow $CoSe_2$ microspheres (956.9 F g^{-1} at 1.0 A g^{-1}), due to the presence of abundant heterogeneous phase interfaces [90]. The ASC depicted in Fig. 9A, which was constructed from $NiSe_2/CoSe_2$ cathode and N,S co-doped rGO aerogel anode ($NiSe_2/CoSe_2$||N,S-rGO), demonstrated a high energy density of 53.7 Wh kg^{-1} at 130.2 W kg^{-1} [90]. To further prove the superior reaction kinetics of the hetero-interfaces compared to monometallic selenides, Yun et al. utilized density functional theory (DFT) calculations [90]. The results indicated that the difference in averaged electrostatic potential between $NiSe_2$ (−33.87 eV) and $CoSe_2$ (−27.46 eV) caused electrons to migrate from $NiSe_2$ to $CoSe_2$, leading to a redistribution of interfacial charges and accumulation of electrons on the $CoSe_2$ side (Fig. 9C) [90]. The depletion of electrons on the $NiSe_2$ side resulted in a strong attraction between OH^- ions from KOH electrolyte and $NiSe_2$ side on the phase boundaries (Fig. 9C), and boosted the rate capability [90]. Additionally, the calculation of OH^- ions adsorption energy revealed that the heterostructured $NiSe_2/CoSe_2$ displayed a lower OH^- ions adsorption energy (−3.33 eV) compared to both $NiSe_2$ (−1.61 eV) and $CoSe_2$ (−1.67 eV), further supporting the enhanced reaction kinetics of the heterogeneous interfaces [90].

In another study, Zardkhoshoui et al. employed structural engineering in heterostructured TMSe to improve the electrochemical properties of nickel-based selenides [13]. They investigated the effect of calcination time on the morphology of the hollow microspheres and found that an increase in the calcination duration resulted in a transformation from a yolk-shell structure to a hollow multi-shell structure, which led to a large surface area with high porosity. Then, they compared the synthesized hollow multi-shelled Ni–Mn–Se microspheres after selenization with Ni–Mn–O, a precursor before selenization, and observed that the former (2035.2 F g^{-1} at 2.0 A g^{-1}) exhibited higher specific capacitance than the latter (1723.8 F g^{-1} at 2.0 A g^{-1}), further demonstrating the superior electrochemical properties of TMSes compared to TMOs. The energy density of the ASC constructed from Ni–Mn–Se||AC was measured as 61.2 Wh kg^{-1} at 804.6 W kg^{-1}, with a cycling stability of 92.6% after 10000 cycles at 32.0 A g^{-1}. It was suggested that the energy density of the ASC could be further improved by substituting the AC anode with other compounds with higher specific capacitance since carbon-based negative electrodes have low specific capacitance and limit the final energy density of ASC. To address this issue, they synthesized hollow double-shelled nickel-iron selenide microspheres, which had higher specific capacitance compared to the AC, and used them as an anode to construct an ASC with the cathode of Ni–Mn–Se, denoted as Ni–Mn–Se||Ni–Fe–Se. The resulting ASC exhibited an exceptional energy density of 112.6 Wh kg^{-1} at 900.8 W kg^{-1} and a higher cycling stability of 94.4% after 10000 cycles at 32.0 A g^{-1}. This study highlights the importance of developing both cathode and anode components in electrochemical energy storage devices and demonstrates the promising potential of TMSe in enabling the development of high energy density ASC.

5.2. Cobalt selenide

Cobalt-based selenides have exhibited good electrochemical performance and can serve as electrodes in supercapacitors [91]. Different types of cobalt-based selenides, including nickel-cobalt [90], copper-cobalt [91], cobalt-molybdenum [41,92], and zinc-cobalt [93] have been studied. As previously mentioned, the morphology of nanoparticles plays a crucial role in the performance of the synthesized compounds [41]. Ma et al. prepared $CoSe_2$–$MoSe_2$ with varying Co:Mo ratios and demonstrated how the ratio affects the active surface area and pore volume resulting more ion/electron transfer routes and a larger contact area between nanoparticles and electrolyte [41]. In their study, the sample with a Co:Mo ratio of 3:1 exhibited the highest performance, achieving a high specific capacitance of 1907.7 F g^{-1} at 1 A g^{-1} [41]. This study emphasizes the significance of optimizing the nanoparticle morphology for achieving high-performance electrodes in supercapacitors [41].

The morphology of nanoparticles can be also modified by controlling the heating rate of annealing. Zardkhoshoui et al. demonstrated the effectiveness of this approach in enhancing the electrochemical performance of TMSes [93]. By using a lower heating rate, the authors were able to allow the elements to diffuse out of the nanoparticles, resulting in a smooth multi-shelled morphology with increased porosity [93]. They synthesized hollow multi-shelled zinc-cobalt-selenide nanospheres wrapped in reduced graphene oxide (rGO) as the cathode to facilitate a fast electron transport path and prevent nanoparticles from aggregation, resulting in a high specific capacitance of 2260.5 F g^{-1} at 2.0 A g^{-1} [93].

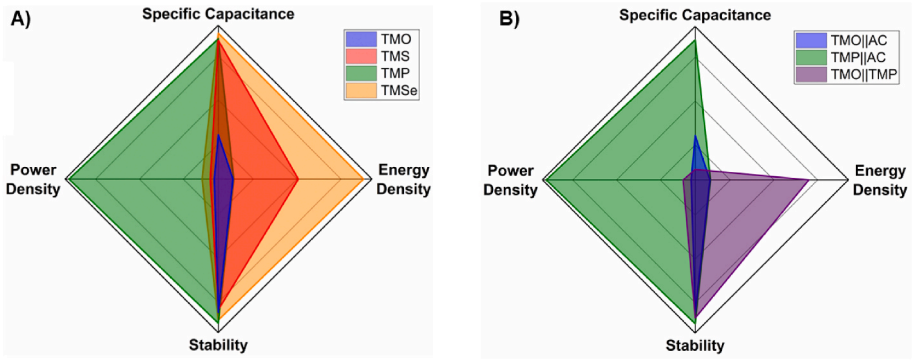

Fig. 11. (A) The electrochemical performance of the supercapacitor selected based on the highest energy density among different types of transition-metal compounds. (B) Comparison between an ASC constructed from TMO||TMP with TMO||AC and TMP||AC supercapacitor.

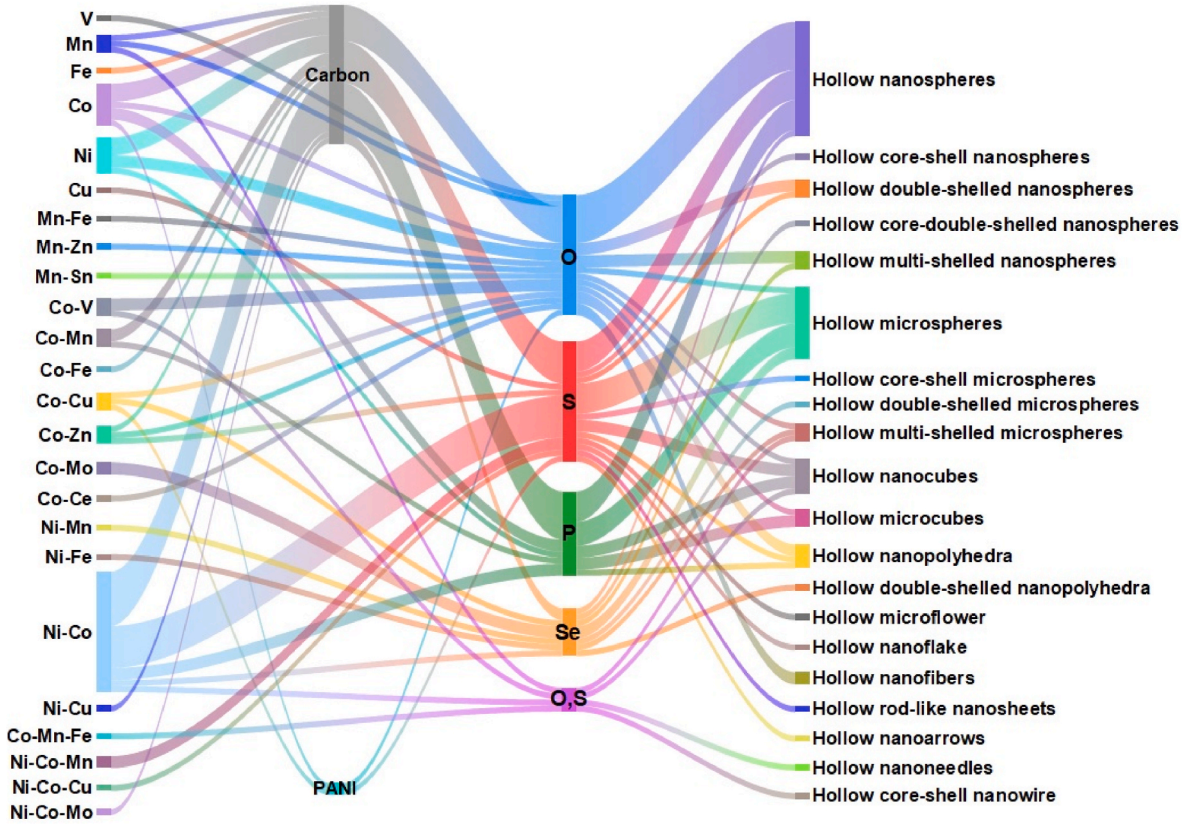

Fig. 12. Quantitative representation of the extent to which each metal, non-metal, and morphology has been investigated, as derived from the literature studied in this review.

In addition, they synthesized hollow yolk-double-shelled cobalt-iron-selenide nanospheres in rGO as the anode to create an ASC from Zn–Co–Se/rGO||Co–Fe–Se/rGO which exhibited an extraordinary energy density of 126.3 Wh kg^{-1} at 902.2 W kg^{-1} [93]. They concluded that controlling the heating rate is another effective way to modify the morphology of nanoparticles and utilizing bimetallic selenides wrapped in rGO as both cathode and anode can lead to a considerable improvement in the energy density of supercapacitors [93].

6. Outlook

In this comprehensive review, the electrochemical performance of transition metal-based hollow micro- and nanoparticles was thoroughly analyzed to determine which type of transition metal-based compound yields the best results. Fig. 10A shows that the specific capacitance of different transition metal compounds is within a similar range, with TMPs exhibiting the highest specific capacitance due to their high theoretical capacitance. Nevertheless, a detailed analysis of TMO, TMS, TMP, and TMSe-based compounds reveals that specific capacitances exceed 2000 F g^{-1} for each material at their maximum performance.

Regarding energy densities, the highest energy density was observed in the TMSe-based supercapacitor constructed from pseudocapacitive cathode and anode, as illustrated in Fig. 10B. The second-highest energy density was achieved in the asymmetric supercapacitors constructed from TMO-based hollow nanoparticles as cathode and TMP-based hollow nanoparticle-based anode. Notably, the highest energy density was not achieved with a carbon-based anode, but rather by implementing other materials in the asymmetric electrodes, as evident from the observation that TMS||AC ASC yielded the lowest energy density.

In order to evaluate the electrochemical performance of transition-

metal based hollow micro- and nanoparticles further, the best-performing samples from each group were compared in terms of their energy density, power density, specific capacitance, and stability, as presented in Fig. 11A. The TMSe-based hollow nanoparticle demonstrated the highest energy density, outperforming all other materials. Notably, the stability of all the materials was similarly high. Furthermore, TMSe-based ASC would still deliver the highest energy density if it operates at the same power density as TMPs. Conversely, TMO and TMP delivered the lowest energy density, but TMP had a higher power density than TMO. In addition, as shown in Fig. 11B, the supercapacitor constructed from TMO as the anode and TMP as the cathode displayed a higher energy density even with lower specific capacitance than the supercapacitors based on TMO or TMP alone, in which active carbon was the anode. This observation highlights the significance of employing transition metal-based materials as both anode and cathode to achieve a high energy density.

Fig. 12 illustrates the distribution of studies across different metals, non-metals, and morphologies of hollow nanoparticles. The results show that studies have been conducted on a broad range of transition metals, with particular attention given to Ni, Co, and bimetallic Ni–Co systems. There have been several studies investigating the incorporation of carbon into the micro- and nanoparticles, with a particular focus on Ni-, Co-, Mn-, NiCo-, and CoMn-based nanoparticles. However, there are only a few studies conducted on the use of polyaniline (PANI), indicating a need for further study in this area. In addition, studies have also focused on non-metals, particularly O and S. With respect to morphology, hollow micro- and nanospheres and hollow micro- and nanocubes are the most studied morphologies followed by hollow multi-shelled micro- and nanospheres and hollow nanopolyhedra. This analysis offers valuable insights into the current research landscape of transition metal-based hollow nanoparticles and sheds light on areas that may require further investigation.

In conclusion, constructing asymmetric supercapacitors from pseudocapacitors (e.g. TMO||TMP) can yield higher energy densities compared to constructing asymmetric supercapacitors from pseudocapacitor and AC (e.g. TMO||AC). However, more research is needed to improve the matching of performance between the two electrodes, which could further enhance the energy density and power density of supercapacitors. This review provided a comprehensive analysis of the electrochemical performance of transition metal-based hollow micro- and nanoparticles, which could aid in the development of high-performance supercapacitors for various energy storage applications.

CRediT authorship contribution statement

Pooria Tajalli: Investigation, Methodology, Validation, Writing – original draft, Writing – review & editing. **Mina Omidiyan:** Investigation, Methodology, Writing – review & editing. **M. Mim Rahimi:** Investigation, Supervision, Writing – review & editing. **T. Randall Lee:** Investigation, Supervision, Writing – review & editing.

Declaration of competing interest

The authors declare that they have no known competing financial interests or personal relationships that could have appeared to influence the work reported in this paper.

Data availability

No data was used for the research described in the article.

Acknowledgments

We thank the Air Force Office of Scientific Research (TRL; AFOSR FA9550-20-1-0349; 20RT0302 and FA9550-23-1-0581; 23RT0567), the Robert A. Welch Foundation (TRL; Grant no. E-1320), the Department of Energy (MR; Award Number: DE-FE-0032408), and the Center for Carbon Management in Energy (CCME) of UH Energy (MR; Award Number: G0509373) for generously supporting this research.

References

[1] G. Harper, R. Sommerville, E. Kendrick, L. Driscoll, P. Slater, R. Stolkin, A. Walton, P. Christensen, O. Heidrich, S. Lambert, A. Abbott, K. Ryder, L. Gaines, P. Anderson, Recycling Lithium-ion batteries from electric vehicles, Nature 575 (2019) 75–86, https://doi.org/10.1038/s41586-019-1682-5.

[2] L. Jiang, Y. Lu, C. Zhao, L. Liu, J. Zhang, Q. Zhang, X. Shen, J. Zhao, X. Yu, H. Li, X. Huang, L. Chen, Y.-S. Hu, Building aqueous K-ion batteries for energy storage, Nat. Energy 4 (2019) 495–503, https://doi.org/10.1038/s41560-019-0388-0.

[3] J. Luo, B. Hu, M. Hu, Y. Zhao, T.L. Liu, Status and prospects of organic redox flow batteries toward sustainable energy storage, ACS Energy Lett. 4 (2019) 2220–2240, https://doi.org/10.1021/acsenergylett.9b01332.

[4] A. Jaradat, C. Zhang, S. Shashikant Sutar, N. Shan, S. Wang, S.K. Singh, T. Yang, K. Kumar, K. Sharma, S. Namvar, A. Alireza, T. Rojas, V. Berry, J. Cabana-Jimenez, Z. Huang, A. Subramanian, A.T. Ngo, L.A. Curtiss, A. Salehi-khojin, A high-rate Li–CO2 battery enabled by 2D medium-entropy catalyst, Adv. Funct. Mater. 33 (2023) 2300814, https://doi.org/10.1002/adfm.202300814.

[5] A. Molaei Aghdam, N.M. Chahartagh, S. Namvar, M. Ershadi, F.B. Ajdari, E. Delfani, Improving the performance of a SnS2 cathode with interspace layer engineering using a Na+ insertion/extraction method for aqueous zinc ion batteries, J. Mater. Chem. A 12 (2024) 1047–1057, https://doi.org/10.1039/D3TA05251F.

[6] A. Molaei Aghdam, S. Habibzadeh, M. Javanbakht, M. Ershadi, M.R. Ganjali, High interspace-layer manganese selenide nanorods as a high-performance cathode for aqueous zinc-ion batteries, ACS Appl. Energy Mater. 6 (2023) 3225–3235, https://doi.org/10.1021/acsaem.2c03621.

[7] P. Aleta, A. Refaie, M. Afshari, A. Hassan, M. Rahimi, Direct Ocean capture: the emergence of electrochemical processes for oceanic carbon removal, Energy Environ. Sci. 16 (2023) 4944–4967, https://doi.org/10.1039/D3EE01471A.

[8] S. Dühnen, J. Betz, M. Kolek, R. Schmuch, M. Winter, T. Placke, Toward green battery cells: perspective on materials and technologies, Small Methods 4 (2020) 2000039, https://doi.org/10.1002/smtd.202000039.

[9] M. Rahimi, Lithium-ion batteries: latest advances and prospects, Batteries 7 (2021), https://doi.org/10.3390/batteries7010008.

[10] J. Luan, H. Yuan, J. Liu, C. Zhong, Recent advances on charge storage mechanisms and optimization strategies of Mn-based cathode in zinc–manganese oxides batteries, Energy Storage Mater. 66 (2024) 103206, https://doi.org/10.1016/j.ensm.2024.103206.

[11] X. Chen, J.-H. Liu, H. Jiang, C. Zhan, Y. Gao, J. Li, H. Zhang, X. Cao, S. Dou, Y. Xiao, Metal organic framework-based cathode materials for aqueous zinc-ion batteries: recent advances and perspectives, Energy Storage Mater. 65 (2024) 103168, https://doi.org/10.1016/j.ensm.2023.103168.

[12] Z. Xue, K. Tao, L. Han, Stringing metal–organic framework-derived hollow Co3S4 nanopolyhedra on V2O5 nanowires for high-performance supercapacitors, Appl. Surf. Sci. 600 (2022) 154076, https://doi.org/10.1016/j.apsusc.2022.154076.

[13] A. Mohammadi Zardkhoshoui, B. Ameri, S.S. Hosseiny Davarani, A high-energy-density supercapacitor with multi-shelled nickel–manganese selenide hollow spheres as cathode and double-shell nickel–iron selenide hollow spheres as anode electrodes, Nanoscale 13 (2021) 2931–2945, https://doi.org/10.1039/D0NR08234A.

[14] L. Wang, F. Liu, A. Pal, Y. Ning, Z. Wang, B. Zhao, R. Bradley, W. Wu, Ultra-small Fe3O4 nanoparticles encapsulated in hollow porous carbon nanocapsules for high performance supercapacitors, Carbon 179 (2021) 327–336, https://doi.org/10.1016/j.carbon.2021.04.024.

[15] J. Cao, Y. Hu, Y. Zhu, H. Cao, M. Fan, C. Huang, K. Shu, M. He, H.C. Chen, Synthesis of mesoporous nickel-cobalt-manganese sulfides as electroactive materials for hybrid supercapacitors, J. Chem. Eng. 405 (2021) 126928, https://doi.org/10.1016/j.cej.2020.126928.

[16] S. Su, L. Sun, J. Qian, X. Shi, Y. Zhang, Hollow bimetallic phosphosulfide NiCo–P/S nanoparticles in a CNT/rGO framework with interface charge redistribution for battery-type supercapacitors, ACS Appl. Energy Mater. 5 (2022) 685–696, https://doi.org/10.1021/acsaem.1c03179.

[17] T. Li, X. Hu, C. Yang, L. Han, K. Tao, A heterostructure of NiMn-LDH nanosheets assembled on ZIF-L-derived ZnCoS hollow nanosheets with a built-in electric field enables boosted electrochemical energy storage, Dalton Trans. 52 (2023) 16640–16649, https://doi.org/10.1039/D3DT02931J.

[18] Z. Song, H. Hu, K. Shu, T. Liu, X. Tang, X. Zhou, Y. Li, Y. Zhang, Novel Fe2O3 microspheres composed of triangular star-shaped nanorods as an electrode for supercapacitors, Chem. Commun. 59 (2023) 11791–11794, https://doi.org/10.1039/D3CC03809B.

[19] M. Rahimi, A. Khurram, T.A. Hatton, B. Gallant, Electrochemical carbon capture processes for mitigation of CO2 emissions, Chem. Soc. Rev. 51 (2022) 8676–8695, https://doi.org/10.1039/D2CS00443G.

[20] S. Deka, Nanostructured mixed transition metal oxide spinels for supercapacitor applications, Dalton Trans. 52 (2023) 839–856, https://doi.org/10.1039/D2DT02733J.

[21] S. Yang, Z. Hao, S. Zhang, Y. Gao, X. Li, J. Peng, L. Li, X. Li, Rational construction of cobalt sulfide nanoparticles embedded in hollow N, P, S codoped carbon shells for enhanced supercapacitor performance, ACS Appl. Energy Mater. 5 (2022) 1436–1446, https://doi.org/10.1021/acsaem.1c02663.

[22] Z. Fahimi, O. Moradlou, A. Sabbah, K.-H. Chen, L.-C. Chen, M. Qorbani, Co3V2O8 hollow spheres with mesoporous walls as high-capacitance electrode for hybrid supercapacitor device, J. Chem. Eng. 436 (2022) 135225, https://doi.org/10.1016/j.cej.2022.135225.
[23] M. Zhong, M. Zhang, X. Li, Carbon nanomaterials and their composites for supercapacitors, Carbon Energy 4 (2022) 950–985, https://doi.org/10.1002/cey2.219.
[24] L. Najmi, Z. Hu, Effects of topological parameters on thermal properties of carbon nanotubes via molecular dynamics simulation, J. Compos. Sci. 8 (2024) 313, https://doi.org/10.3390/jcs8010037.
[25] L. Najmi, Z. Hu, Effects of carbon nanotubes on thermal behavior of epoxy resin composites, J. Compos. Sci. (2023) 7, https://doi.org/10.3390/jcs7080313.
[26] W. Lu, M. Yang, X. Jiang, Y. Yu, X. Liu, Y. Xing, Template-assisted synthesis of hierarchically hollow C/NiCo2S4 nanospheres electrode for high performance supercapacitors, J. Chem. Eng. 382 (2020) 122943, https://doi.org/10.1016/j.cej.2019.122943.
[27] N.K. Mishra, R. Mondal, P. Singh, Synthesis, characterizations and electrochemical performances of anhydrous CoC2O4 nanorods for pseudocapacitive energy storage applications, RSC Adv. 11 (2021) 33926–33937, https://doi.org/10.1039/D1RA05180F.
[28] Y. Gogotsi, R.M. Penner, Energy storage in nanomaterials – capacitive, pseudocapacitive, or battery-like? ACS Nano 12 (2018) 2081–2083, https://doi.org/10.1021/acsnano.8b01914.
[29] C. Huang, S. Lv, A. Gao, J. Ling, F. Yi, J. Hao, M. Wang, Z. Luo, D. Shu, Boosting the energy density of supercapacitors by designing both hollow NiO nanoparticles/nitrogen-doped carbon cathode and nitrogen-doped carbon anode from the same precursor, J. Chem. Eng. 431 (2022) 134083, https://doi.org/10.1016/j.cej.2021.134083.
[30] C. Kang, L. Ma, Y. Chen, L. Fu, Q. Hu, C. Zhou, Q. Liu, Metal-organic framework derived hollow rod-like NiCoMn ternary metal sulfide for high-performance asymmetric supercapacitors, J. Chem. Eng. 427 (2022) 131003, https://doi.org/10.1016/j.cej.2021.131003.
[31] M. Amiri, S.E. Moosavifard, S.S.H. Davarani, S.K. Kaverlavani, M. Shamsipur, MnCoP hollow nanocubes as novel electrode material for asymmetric supercapacitors, J. Chem. Eng. 420 (2021) 129910, https://doi.org/10.1016/j.cej.2021.129910.
[32] Y. Du, G. Li, M. Chen, X. Yang, L. Ye, X. Liu, L. Zhao, Hollow nickel-cobalt-manganese hydroxide polyhedra via MOF templates for high-performance quasi-solid-state supercapacitor, J. Chem. Eng. 378 (2019) 122210, https://doi.org/10.1016/j.cej.2019.122210.
[33] A. Ehsani, A.A. Heidari, H.M. Shiri, Electrochemical pseudocapacitors based on ternary nanocomposite of conductive polymer/graphene/metal oxide: an introduction and review to it in recent studies, Chem. Rec. 19 (2019) 908–926, https://doi.org/10.1002/tcr.201800112.
[34] X. Ren, H. Fan, J. Ma, C. Wang, M. Zhang, N. Zhao, Hierarchical Co3O4/PANI hollow nanocages: synthesis and application for electrode materials of supercapacitors, Appl. Surf. Sci. 441 (2018) 194–203, https://doi.org/10.1016/j.apsusc.2018.02.013.
[35] T. Zhao, C. Liu, F. Yi, W. Deng, A. Gao, D. Shu, L. Zheng, Hollow N-doped carbon @ O-vacancies NiCo2O4 nanocages with a built-in electric field as high-performance cathodes for hybrid supercapacitor, Electrochim. Acta 364 (2020) 137260, https://doi.org/10.1016/j.electacta.2020.137260.
[36] F.H. Likhi, M. Singh, S.V. Chavan, T. Cao, M. Shanbedi, A. Karim, Effects of film confinement on dielectric and electrical properties of graphene oxide and reduced graphene oxide-based polymer nanocomposites: implications for energy storage, ACS Appl. Nano Mater. 6 (2023) 11699–11714, https://doi.org/10.1021/acsanm.3c01674.
[37] M. Shanbedi, H. Ardebili, A. Karim, Polymer-based triboelectric nanogenerators: materials, characterization, and applications, Prog. Polym. Sci. 144 (2023) 101723, https://doi.org/10.1016/j.progpolymsci.2023.101723.
[38] L. Najmi, Z. Hu, Review on molecular dynamics simulations of effects of carbon nanotubes (CNTs) on electrical and thermal conductivities of CNT-modified polymeric composites, J. Compos. Sci. 7 (2023) 165, https://doi.org/10.3390/jcs7040165.
[39] Lida Najmi, S.M. Zebarjad, K. Janghorban, Effects of carbon nanotubes on the compressive and flexural strength and microscopic structure of epoxy honeycomb sandwich panels, Polym. Sci. Ser. B 65 (2023) 220–229, https://doi.org/10.1134/S1560090423700872.
[40] K. Xu, S. Li, J. Yang, J. Hu, Hierarchical hollow MnO2 nanofibers with enhanced supercapacitor performance, J. Colloid Interface Sci. 513 (2018) 448–454, https://doi.org/10.1016/j.jcis.2017.11.052.
[41] F. Ma, J. Lu, L. Pu, W. Wang, Y. Dai, Construction of hierarchical cobalt-molybdenum selenide hollow nanospheres architectures for high performance battery-supercapacitor hybrid devices, J. Colloid Interface Sci. 563 (2020) 435–446, https://doi.org/10.1016/j.jcis.2019.12.101.
[42] P. Makkar, N.N. Ghosh, Facile synthesis of MnFe2O4 hollow sphere-reduced graphene oxide nanocomposites as electrode materials for all-solid-state flexible high-performance asymmetric supercapacitors, ACS Appl. Energy Mater. 3 (2020) 2653–2664, https://doi.org/10.1021/acsaem.9b02360.
[43] E. Niknam, H. Naffakh-Moosavy, S.E. Moosavifard, M.G. Afshar, Multi-shelled bimetal V-doped Co3O4 hollow spheres derived from metal organic framework for high performance supercapacitors, J. Energy Storage 44 (2021) 103508, https://doi.org/10.1016/j.est.2021.103508.
[44] Z. Wang, H. Jia, Y. Cai, C. Li, X. Zheng, H. Liang, J. Qi, J. Cao, J. Feng, Highly conductive Mn3O4/MnS heterostructures building multi-shelled hollow microspheres for high-performance supercapacitors, J. Chem. Eng. 392 (2020) 123890, https://doi.org/10.1016/j.cej.2019.123890.
[45] A. Mohammadi Zardkhoshoui, B. Ameri, S. Saeed Hosseiny Davarani, Fabrication of hollow MnFe2O4 nanocubes assembled by CoS2 nanosheets for hybrid supercapacitors, J. Chem. Eng. 435 (2022) 135170, https://doi.org/10.1016/j.cej.2022.135170.
[46] B.P. Reddy, K. Mallikarjuna, M. Kumar, M.C. Sekhar, Y. Suh, S.-H. Park, Highly porous metal organic framework derived NiO hollow spheres and flowers for oxygen evolution reaction and supercapacitors, Ceram. Int. 47 (2021) 3312–3321, https://doi.org/10.1016/j.ceramint.2020.09.172.
[47] H. Jia, J. Fan, Z. Huo, L. Wang, Z. Wang, C. Feng, H. Jin, M.-C. Liu, In situ encapsulation hollow FeP spheres into high yield 3D N, P-codoped graphenic framework as advanced anode material for high-performance supercapacitors, J. Alloys Compd. 924 (2022) 166603, https://doi.org/10.1016/j.jallcom.2022.166603.
[48] X. Jing, Y. Zhang, H. Jiang, Y. Cheng, N. Xing, C. Meng, Facile template-free fabrication of hierarchical V2O5 hollow spheres with excellent charge storage performance for symmetric and hybrid supercapacitor devices, J. Alloys Compd. 763 (2018) 180–191, https://doi.org/10.1016/j.jallcom.2018.05.303.
[49] M. Wu, C. Chen, J. Zhou, F. Yi, K. Tao, L. Han, MOF–Derived hollow double–shelled NiO nanospheres for high–performance supercapacitors, J. Alloys Compd. 734 (2018) 1–8, https://doi.org/10.1016/j.jallcom.2017.10.171.
[50] C. Wang, J. Wang, W. Hu, D. Wang, Controllable synthesis of hollow multishell structured Co3O4 with improved rate performance and cyclic stability for supercapacitors, Chem. Res. Chin. Univ. 36 (2020) 68–73, https://doi.org/10.1007/s40242-019-0040-3.
[51] T. Liu, L. Zhang, W. You, J. Yu, Core–shell nitrogen-doped carbon hollow spheres/Co3O4 nanosheets as advanced electrode for high-performance supercapacitor, Small 14 (2018) 1702407, https://doi.org/10.1002/smll.201702407.
[52] Y. Yan, L. Zang, T. Dou, H. Li, L. Sun, Y. Zhang, Hollow Co3O4 nanoparticles immobilized rGO/carbon monolith as an electrode material for high-performance supercapacitors, Ceram. Int. 47 (2021) 20310–20316, https://doi.org/10.1016/j.ceramint.2021.04.039.
[53] Y. Shang, T. Xie, C. Ma, L. Su, Y. Gai, J. Liu, L. Gong, Synthesis of hollow ZnCo2O4 microspheres with enhanced electrochemical performance for asymmetric supercapacitor, Electrochim. Acta 286 (2018) 103–113, https://doi.org/10.1016/j.electacta.2018.08.025.
[54] C. Wei, K. Liu, J. Tao, X. Kang, H. Hou, C. Cheng, D. Zhang, Self-template synthesis of hybrid porous Co3O4–CeO2 hollow polyhedrons for high-performance supercapacitors, Chem. Asian J. 13 (2018) 111–117, https://doi.org/10.1002/asia.201701582.
[55] F. Saleki, A. Mohammadi, S.E. Moosavifard, A. Hafizi, M.R. Rahimpour, MOF assistance synthesis of nanoporous double-shelled CuCo2O4 hollow spheres for hybrid supercapacitors, J. Colloid Interface Sci. 556 (2019) 83–91, https://doi.org/10.1016/j.jcis.2019.08.044.
[56] W. Feng, G. Liu, P. Wang, J. Zhou, L. Gu, L. Chen, X. Li, Y. Dan, X. Cheng, Template synthesis of a heterostructured MnO2@SnO2 hollow sphere composite for high asymmetric supercapacitor performance, ACS Appl. Energy Mater. 3 (2020) 7284–7293, https://doi.org/10.1021/acsaem.0c00388.
[57] H. Yun, X. Zhou, H. Zhu, M. Zhang, One-dimensional zinc-manganate oxide hollow nanostructures with enhanced supercapacitor performance, J. Colloid Interface Sci. 585 (2021) 138–147, https://doi.org/10.1016/j.jcis.2020.11.060.
[58] Y. Ma, L. Zhang, Z. Yan, B. Cheng, J. Yu, T. Liu, Sandwich-shell structured CoMn2O4/C hollow nanospheres for performance-enhanced sodium-ion hybrid supercapacitor, Adv. Energy Mater. 12 (2022) 2103820, https://doi.org/10.1002/aenm.202103820.
[59] M. Rahimi, G. Catalini, S. Hariharan, M. Wang, M. Puccini, T.A. Hatton, Carbon dioxide capture using an electrochemically driven proton concentration process, Cell Rep. Phys. Sci. 1 (2020) 100033, https://doi.org/10.1016/j.xcrp.2020.100033.
[60] M. Rahimi, G. Catalini, M. Puccini, T.A. Hatton, Bench-scale demonstration of CO2 capture with an electrochemically driven proton concentration process, RSC Adv. 10 (29) (2020) 16832–16843, https://doi.org/10.1039/D0RA02450C.
[61] J. Zhang, Y. Deng, Y. Wu, Z. Xiao, X. Liu, Z. Li, R. Bu, Q. Zhang, W. Sun, L. Wang, Chemically coupled 0D-3D hetero-structure of Co9S8-Ni3S4 hollow spheres for Zn-based supercapacitors, J. Chem. Eng. 430 (2022) 132836, https://doi.org/10.1016/j.cej.2021.132836.
[62] Q. Li, W. Lu, Z. Li, J. Ning, Y. Zhong, Y. Hu, Hierarchical MoS2/NiCo2S4@C urchin-like hollow microspheres for asymmetric supercapacitors, J. Chem. Eng. 380 (2020) 122544, https://doi.org/10.1016/j.cej.2019.122544.
[63] X. Yu, J. Yu, L. Hou, A. Gagnoud, Y. Fautrelle, Z. Ren, X. Li, Double-shelled hollow hetero-MnCo2S4/CoS1.097 spheres with carbon coating for advanced supercapacitors, J. Power Sources 408 (2018) 65–73, https://doi.org/10.1016/j.jpowsour.2018.10.082.
[64] P. Cai, T. Liu, L. Zhang, B. Cheng, J. Yu, ZIF-67 derived nickel cobalt sulfide hollow cages for high-performance supercapacitors, Appl. Surf. Sci. 504 (2020) 144501, https://doi.org/10.1016/j.apsusc.2019.144501.
[65] Y. Liu, Z. Zhou, S. Zhang, W. Luo, G. Zhang, Controllable synthesis of CuS hollow microflowers hierarchical structures for asymmetric supercapacitors, Appl. Surf. Sci. 442 (2018) 711–719, https://doi.org/10.1016/j.apsusc.2018.02.220.
[66] C. Huang, A. Gao, F. Yi, Y. Wang, D. Shu, Y. Liang, Z. Zhu, J. Ling, J. Hao, Metal organic framework derived hollow NiS@C with S-vacancies to boost high-performance supercapacitors, J. Chem. Eng. 419 (2021) 129643, https://doi.org/10.1016/j.cej.2021.129643.
[67] Y. Cui, J. Zhang, C. Jin, Y. Liu, W. Luo, W. Zheng, Ionic liquid-controlled growth of NiCo2S4 3D hierarchical hollow nanoarrow arrays on Ni foam for superior

performance binder free hybrid supercapacitors, Small 15 (2019) 1804318, https://doi.org/10.1002/smll.201804318.
[68] Y. Gao, B. Wu, J. Hei, D. Gao, X. Xu, Z. Wei, H. Wu, Self-assembled synthesis of waxberry-like open hollow NiCo2S4 with enhanced capacitance for high-performance hybrid asymmetric supercapacitors, Electrochim. Acta 347 (2020) 136314, https://doi.org/10.1016/j.electacta.2020.136314.
[69] C. Wei, N. Zhan, J. Tao, S. Pang, L. Zhang, C. Cheng, D. Zhang, Synthesis of hierarchically porous NiCo2S4 core-shell hollow spheres via self-template route for high performance supercapacitors, Appl. Surf. Sci. 453 (2018) 288–296, https://doi.org/10.1016/j.apsusc.2018.05.003.
[70] L. Chen, J. Wan, L. Fan, Y. Wei, J. Zou, Construction of CoNi2S4 hollow cube structures for excellent performance asymmetric supercapacitors, Appl. Surf. Sci. 570 (2021) 151174, https://doi.org/10.1016/j.apsusc.2021.151174.
[71] X. Han, Q. Chen, H. Zhang, Y. Ni, L. Zhang, Template synthesis of NiCo2S4/Co9S8 hollow spheres for high-performance asymmetric supercapacitors, J. Chem. Eng. 368 (2019) 513–524, https://doi.org/10.1016/j.cej.2019.02.138.
[72] Y. Liu, G. Jiang, Z. Huang, Q. Lu, B. Yu, U. Evariste, P. Ma, Decoration of hollow mesoporous carbon spheres by NiCo2S4 nanoparticles as electrode materials for asymmetric supercapacitors, ACS Appl. Energy Mater. 2 (2019) 8079–8089, https://doi.org/10.1021/acsaem.9b01569.
[73] S.G. Mohamed, I. Hussain, J.-J. Shim, One-step synthesis of hollow C-NiCo2S4 nanostructures for high-performance supercapacitor electrodes, Nanoscale 10 (2018) 6620–6628, https://doi.org/10.1039/C7NR07338K.
[74] F. Zhu, W. Liu, Y. Liu, W. Shi, Self-supported hierarchical core–shell Co9S8@ NiCo2O4 hollow nanoneedle arrays for asymmetric supercapacitors, Inorg. Chem. Front. 6 (2019) 982–987, https://doi.org/10.1039/C9QI00117D.
[75] M. Abuali, N. Arsalani, I. Ahadzadeh, T. Nann, Synthesis of CuCo2S4 nanoparticles assembled in micro-sized hollow spheres composed with polyaniline: an effective electrode material for supercapacitors, Mater. Sci. Eng. B. 276 (2022) 115578, https://doi.org/10.1016/j.mseb.2021.115578.
[76] C. Cheng, X. Zhang, C. Wei, Y. Liu, C. Cui, Q. Zhang, D. Zhang, Mesoporous hollow ZnCo2S4 core-shell nanospheres for high performance supercapacitors, Ceram. Int. 44 (2018) 17464–17472, https://doi.org/10.1016/j.ceramint.2018.06.215.
[77] W. Zhao, G. Yan, Y. Zheng, B. Liu, D. Jia, T. Liu, L. Cui, R. Zheng, D. Wei, J. Liu, Bimetal-organic framework derived Cu(NiCo)2S4/Ni3S4 electrode material with hierarchical hollow heterostructure for high performance energy storage, J. Colloid Interface Sci. 565 (2020) 295–304, https://doi.org/10.1016/j.jcis.2020.01.049.
[78] C. Wei, Q. Chen, C. Cheng, R. Liu, Q. Zhang, L. Zhang, Mesoporous nickel cobalt manganese sulfide yolk–shell hollow spheres for high-performance electrochemical energy storage, Inorg. Chem. Front. 6 (2019) 1851–1860, https://doi.org/10.1039/C9QI00173E.
[79] X. Zhang, L. Zhang, G. Xu, A. Zhao, S. Zhang, T. Zhao, Template synthesis of structure-controlled 3D hollow nickel-cobalt phosphides microcubes for high-performance supercapacitors, J. Colloid Interface Sci. 561 (2020) 23–31, https://doi.org/10.1016/j.jcis.2019.11.112.
[80] Z. Xiao, Y. Bao, Z. Li, X. Huai, M. Wang, P. Liu, L. Wang, Construction of hollow cobalt–nickel phosphate nanocages through a controllable etching strategy for high supercapacitor performances, ACS Appl. Energy Mater. 2 (2019) 1086–1092, https://doi.org/10.1021/acsaem.8b01627.
[81] X. Ma, J. Chen, B. Yuan, Y. Li, L. Yu, W. Zhao, Three-dimensional hollow nickel phosphate microspheres with controllable hoya-like structure for high-performance enzymeless glucose detection and supercapacitor, Appl. Surf. Sci. 588 (2022) 152928, https://doi.org/10.1016/j.apsusc.2022.152928.
[82] S. Liu, Y. Xu, C. Wang, Y. An, Metal-organic framework derived Ni2P/C hollow microspheres as battery-type electrodes for battery-supercapacitor hybrids, Chemelectrochem 6 (2019) 5511–5518, https://doi.org/10.1002/celc.201901504.
[83] L. Ding, K. Zhang, L. Chen, Z. Yu, Y. Zhao, G. Zhu, G. Chen, D. Yan, H. Xu, A. Yu, Formation of three-dimensional hierarchical pompon-like cobalt phosphide hollow microspheres for asymmetric supercapacitor with improved energy density, Electrochim. Acta 299 (2019) 62–71, https://doi.org/10.1016/j.electacta.2018.12.180.
[84] W. Wang, L. Zhang, G. Xu, H. Song, L. Yang, C. Zhang, J. Xu, D. Jia, Structure-designed synthesis of CoP microcubes from metal–organic frameworks with enhanced supercapacitor properties, Inorg. Chem. 57 (2018) 10287–10294, https://doi.org/10.1021/acs.inorgchem.8b01524.
[85] X. Chen, Y. Sun, W. Liu, Template-assisted synthesized hollow sphere-like NiCoP/carbon nanoparticles composites for high-performance asymmetric supercapacitors, J. Electroanal. Chem. 880 (2021) 114862, https://doi.org/10.1016/j.jelechem.2020.114862.
[86] T. Zhao, C. Liu, F. Yi, X. Liu, A. Gao, D. Shu, J. Ling, Promoting high-energy supercapacitor performance over NiCoP/N-doped carbon hybrid hollow nanocages via rational architectural and electronic modulation, Appl. Surf. Sci. 569 (2021) 151098, https://doi.org/10.1016/j.apsusc.2021.151098.
[87] M. Yi, B. Lu, X. Zhang, Y. Tan, Z. Zhu, Z. Pan, J. Zhang, Ionic liquid-assisted synthesis of nickel cobalt phosphide embedded in N, P codoped-carbon with hollow and folded structures for efficient hydrogen evolution reaction and supercapacitor, Appl. Catal. B Environ. 283 (2021) 119635, https://doi.org/10.1016/j.apcatb.2020.119635.
[88] T. Dong, X. Zhang, P. Wang, H.-S. Chen, P. Yang, Hierarchical nickel-cobalt phosphide hollow spheres embedded in P-doped reduced graphene oxide towards superior electrochemistry activity, Carbon 149 (2019) 222–233, https://doi.org/10.1016/j.carbon.2019.04.050.
[89] M. Amiri, A. Mohammadi Zardkhoshoui, S.S. Hosseiny Davarani, Fabrication of nanosheet-assembled hollow copper–nickel phosphide spheres embedded in reduced graphene oxide texture for hybrid supercapacitors, Nanoscale 15 (2023) 2806–2819, https://doi.org/10.1039/D2NR06305K.
[90] X. Yun, T. Lu, R. Zhou, Z. Lu, J. Li, Y. Zhu, Heterostructured NiSe2/CoSe2 hollow microspheres as battery-type cathode for hybrid supercapacitors: electrochemical kinetics and energy storage mechanism, J. Chem. Eng. 426 (2021) 131328, https://doi.org/10.1016/j.cej.2021.131328.
[91] S.E. Moosavifard, F. Saleki, A. Mohammadi, A. Hafizi, M.R. Rahimpour, Construction of hierarchical nanoporous bimetallic copper-cobalt selenide hollow spheres for hybrid supercapacitor, J. Electroanal. Chem. 871 (2020) 114295, https://doi.org/10.1016/j.jelechem.2020.114295.
[92] M. Amiri, S. Saeed Hosseiny Davarani, S. Ebrahim Moosavifard, Y.-Q. Fu, Cobalt-molybdenum selenide double-shelled hollow nanocages derived from metal-organic frameworks as high performance electrodes for hybrid supercapacitor, J. Colloid Interface Sci. 616 (2022) 141–151, https://doi.org/10.1016/j.jcis.2022.02.063.
[93] A. Mohammadi Zardkhoshoui, S.S. Hosseiny Davarani, Boosting the energy density of supercapacitors by encapsulating a multi-shelled zinc–cobalt-selenide hollow nanosphere cathode and a yolk–double shell cobalt–iron-selenide hollow nanosphere anode in a graphene network, Nanoscale 12 (2020) 12476–12489, https://doi.org/10.1039/D0NR02642E.
[94] P. Hassan, A. Aleta, M. Refaie, Y. Afshari, E. Fang, M. Kalantari, Rahimi, Reviving the Absorbent Chemistry of Electrochemically Mediated Amine Regeneration for Improved Carbon Capture Form Flue Gas, Chemical Engineering Journal 484 (2024) 149566.
[95] K. Chowdhury, S. Behura, M. Rahimi, M. Heydari G, °CVD PEDOT-Cl Thin Film Grown by SbCl5 Oxidant as the Hole Transport Layer to Enhance the Perovskite Solar Cell Device Stability, ACS Applied Energy Materials 7 (2024) 1068–1079.